Neuroendocrine control of the proteostatic network by HPK-1 delays aging

Authors: Maria I. Lazaro-Pena[1], Carlos A. Diaz-Balzac[2], Ritika Das[1,3,4], Andrew V. Samuelson[1*]

Affiliations:

[1] Department of Biomedical Genetics, University of Rochester Medical Center, Rochester, New York, USA

[2] Division of Endocrinology, Diabetes and Metabolism, Department of Medicine, University of Rochester Medical Center, Rochester, New York, USA

[3] Department of Biology, University of Rochester, Rochester, New York, USA

[4] Department of Cell Biology, Skirball Institute of Biomolecular Medicine, NYU School of Medicine, New York, New York, USA.

* Corresponding author. Andrew_Samuelson@URMC.Rochester.edu

Author Contributions: M.I.L.P. designed, conducted, and analyzed the majority of experiments. C.A.D.B. assisted in the completion of multiple experiments. R.D. designed and conducted the experiments in Fig 1A, F. A.V.S. oversaw the project from concept to completion, contributing primarily to experimental design and the analysis and interpretation of results. M.I.L.P. and A.V.S. wrote the manuscript.

Competing Interest Statement: The authors have no competing interests.

Classification: Biological Sciences. Cell biology. Genetics. Neuroscience.

Keywords: Neuronal cell-nonautonomous control, proteostasis, longevity, stress response and autophagy

Abstract

The nervous system systemically coordinates proteostasis to delay organismal aging. However, the neuronal regulatory mechanisms that coordinate cellular anti-aging programs across tissue and cell-types are relatively unknown. In this work, we identify the homeodomain-interacting protein kinase (HPK-1), a transcriptional cofactor, as a novel neuronal component of the proteostatic network: its overexpression produces a paracrine signal to hyper-induce molecular chaperones and a neuroendocrine signal to induce autophagy in peripheral tissues. Neuronal HPK-1 signaling improves proteostasis in distal tissues through neurotransmitters. These pro-longevity modalities are independently regulated within serotonergic and GABAergic neurons, respectively, through distinct adaptive responses, either of which improve proteostasis in a cell non-autonomous manner. Serotonergic HPK-1 activity amplifies the heat shock response and protects the proteome from acute stress, without altering longevity. Conversely, increased GABAergic HPK-1 activity is sufficient to induce autophagy and extend longevity, without altering acute stress survival. Consistently, GABAergic neurons, but not serotonin, is essential for the cell non-autonomous induction of autophagy by neuronal HPK-1. These findings provide novel insight into how the nervous system partitions and coordinates unique adaptive response pathways to delay organismal aging, and reveals a key role for neuronal HPK-1 in regulating the proteostatic network throughout an intact metazoan animal.

Significance Statement

Aging and the age-associated decline of the proteome is determined in part through neuronal control of evolutionarily conserved transcriptional effectors, which safeguard homeostasis under fluctuating metabolic and stress conditions by regulating an expansive proteostatic network in peripheral tissues. How neuronal signaling mechanisms are primed, relayed through an organism, and specific responses are initiated in receiving cell types remain poorly understood. We have discovered that the *Caenorhabditis elegans* homeodomain-interacting protein kinase (HPK-1) is a novel transcriptional effector that functions within two distinct neuronal cell-types to non-

autonomously regulate divergent components of the proteostatic network to enhance stress resistance, improve proteostasis and delay aging.

Main Text

Introduction

Cellular aging throughout an organism is characterized by the gradual decline of function within the proteome (proteostasis), which precipitates the onset and progression of a growing number of age-associated diseases both within and outside of the nervous system (1-9). A growing number of studies suggest that aging is not simply the result of the stochastic accumulation of damage, but is determined through genetics and coordinated mechanisms across tissues and cell types (10-12). This is not to say that aging or proteostatic decline occurs through a predetermined "clock"; rather genetic variation predisposes some individuals to age well and others to age poorly. Proteostatic decline corresponds with the age-associated breakdown of a large proteostasis network (PN), which coordinates stress-responsive control of protein folding, degradation, and translation in response to myriad cell intrinsic and non-autonomous signals. And yet, while major components and regulators of the proteostatic network have been identified, it is still poorly understood how multi-cellular organisms coordinate the maintenance of proteostasis across tissues to delay aging.

The relatively simple metazoan animal *Caenorhabditis elegans* (*C. elegans*) is a premiere model system for discovering how proteostasis is coordinated across cell- and tissue- types in response to myriad signals, and how these homeostatic processes breakdown during normal aging. The ability to examine complex cell non-autonomous regulatory interactions are derived from an invariant cell-lineage, a simplified nervous system, powerful tools to dissect cell- and tissue- type genetic interactions, a wealth of both genetic mutants and molecular/cellular reporters of the proteostatic network, and well characterized, quantifiable markers of age-associated decline in the proteome (12, 13). Discoveries of cell non-autonomous signaling first made in *C. elegans* are increasingly being demonstrated to have evolutionarily conserved components (14), which

suggests overarching biological principles and mechanisms exist in how metazoans maintain proteostasis, and how they fail during normal aging.

An increasing number of studies have revealed the nervous system as a key cell non-autonomous regulator of organismal proteostasis and longevity in *C. elegans* (reviewed in (14)). For example, a pair of thermosensory neurons regulate the heat shock response (HSR) in distal tissue in a serotonin-dependent manner (15, 16). In contrast, a second regulatory component from the GABAergic and cholinergic system normally limits muscle cell proteostasis (17, 18). Interestingly, neuronal overexpression of heat shock transcription factor 1 (HSF-1) increases stress resistance and longevity through separable mechanisms (19). In accordance to these findings, another study found that integrin-linked kinase (ILK) inhibition activates HSF-1 cell non-autonomous effects on stress resistance and lifespan in a thermosensory-dependent manner (20). These studies highlight the key role of neuronal signaling in the regulation of proteostasis in distal tissues. Despite these advances, how neuronal cell non-autonomous signaling is activated under different adaptive cellular responses to metabolic and acute stress upon the proteome remains largely unknown.

In *C. elegans,* the transcriptional co-factor homeodomain-interacting protein kinase (HPK-1), preserves proteostasis and organismal longevity (21-23). We have previously shown that HPK-1 extends longevity and delays age-associated decline in proteostasis through distinct genetic pathways defined by the heat shock transcription factor (HSF-1), and the target of rapamycin complex 1 (TORC1) (23). Activation by either metabolic or genotoxic stressors has been observed from yeast to mammals, suggesting that this family of transcriptional cofactors arose early in evolution to couple metabolic and stress signaling (24-27).

The mammalian Hipk family consists of four conserved kinases (Hipk1-4), functioning as transcriptional co-factors that regulate cell growth, development, differentiation and apoptosis (28, 29). In general, HIPK family members regulate the activity of transcription factors, chromatin modifiers, signaling molecules and scaffolding proteins in response to cellular stress; including the

DNA damage response, hypoxia response, reactive oxygen species (ROS), glucose availability, and viral infection (28, 30-32). For example, genotoxic damage induces mammalian *Hipk2,* and HIPK2 potentiates p53 pro-apoptotic activity through direct phosphorylation (24). Nutrient stress, such as glucose deprivation can also activate Hipk1, as well as Hipk2 (32-34). Conversely, hyperglycemia triggers HIPK2 degradation via the proteasome (35).

We sought to identify the tissue- and cell-types in which the HPK-1 transcriptional circuits acts, and how signals and regulatory components are coordinated and integrated across tissues to determine organismal longevity. We have discovered that HPK-1 functions as a key regulator of the proteostatic response, originating in the nervous system of *C. elegans*. HPK-1 acts in the nervous system to stimulate the release of both paracrine and endocrine signals that cell non-autonomously trigger protective peripheral responses. These responses can qualitatively differ depending on the neuronal type from which they arise. Serotonergic HPK-1 activity increases thermotolerance and protects the proteome from acute stress by hyper-induction of the heat shock response, without increasing lifespan or altering basal autophagy. In contrast, GABAergic HPK-1 activity fortifies the proteome by inducing autophagy to extend longevity, without altering thermotolerance. Yet, each of these distinct adaptive responses improves proteostasis in non-neuronal tissues. Our findings reveal HPK-1 as a novel neuronal regulator that coordinates adaptive metabolic and stress response pathways across tissues to delay aging throughout an animal.

Results

HPK-1 acts from neuronal tissue to promote longevity and health span.

Organismal longevity is dependent upon the continued fidelity of a growing number of homeostatic mechanisms, which often have distinct spatial and temporal regulation. We sought to determine where HPK-1 exerts a regulatory control of longevity. We previously found that loss of *hpk-1* solely within either neuronal, intestinal, or hypodermal cells is sufficient to shorten lifespan

(23). However, while *hpk-1* null-mutant animals are viable and fertile, HPK-1 and orthologs are known to have roles in development, differentiation and cell fate-specification (28, 29, 36-39). Thus, even though *hpk-1* null mutants display signs of premature aging and *hpk-1* overexpression throughout the soma extends longevity (23), it is possible that loss of *hpk-1* in some tissues may shorten adult lifespan by subtle developmental deficiencies independent of a role in aging.

To precisely determine where HPK-1 functions in the regulation of longevity, we overexpressed *hpk-1* in different tissues to identify where activity was sufficient to increase lifespan. We expressed *hpk-1* cDNA in either neuronal, muscle, intestine or hypodermis using well characterized tissue specific promoters (*rab-3p::hpk-1, myo-3p::hpk-1, ges-1p::hpk-1* and *dpy-7p::hpk-1*, respectively*)*. Transgenic animals overexpressing *hpk-1* in either muscular, intestinal, or hypodermal cells had a normal lifespan (Fig 1B-D). In contrast, neuronal overexpression of *hpk-1* was sufficient to significantly increase lifespan by 17%, a modest amount comparable to constitutive overexpression of *hpk-1* throughout the soma (Fig. 1A) (23).

Because *hpk-1* null mutant animals are short-lived, and aging correlates with decreased movement (21-23, 40, 41), we performed a locomotion assay. *hpk-1(pk1393)* null mutants displayed a reduced number of body bends at day 2 of adulthood (Fig. 1E). However, overexpression of *hpk-1* in neurons was sufficient to mitigate the locomotion defect of *hpk-1* null mutants. We and others previously found that in the absence of *hpk-1*, animals are vulnerable to acute thermal stress (22, 23). Restoring *hpk-1* expression solely within the nervous system was sufficient to fully rescue the reduced thermotolerance of *hpk-1* null mutant day 1 adult animals (Fig. 1F). We conclude that *hpk-1* primarily acts within the nervous system to promote longevity, health span, and thermal stress resistance.

Neuronal HPK-1 regulates muscle proteostasis via neurotransmission.

The observed beneficial role of neuronal HPK-1 to extend longevity led us to postulate whether neuronal HPK-1 activates a cell extrinsic signal to regulate proteostasis in distal tissues. To investigate whether HPK-1 activity in neurons regulates distal muscle proteostasis, we used a

proteostasis reporter expressed exclusively in muscle tissue (*unc-54p::Q35::YFP*) (42). Animals with increased neuronal *hpk-1* expression had significantly decreased fluorescent foci in muscle tissue (Fig. 2A*i-ii*). For instance, at day 3 of adulthood, animals overexpressing neuronal HPK-1 had an average of 21 ± 0.9 polyQ aggregates, while control animals had an average of 26 ± 1.1 polyQ aggregates (Fig. 2B). In *C. elegans*, the age-related progressive proteotoxic stress of muscle polyQ expression is pathological and results in paralysis. Of note, *hpk-1* overexpression in neurons was sufficient to reduce paralysis; at day 13 of adulthood only 61% ± 0.10 of neuronal *hpk-1* overexpressing animals were paralyzed compared to 81% ± 0.08 of paralyzed control animals (Fig. 2C).

We next tested whether neuronal HPK-1 is required for maintaining muscle proteostasis. The nervous system of wild-type *C. elegans* is largely refractory to RNAi, as these cells do not express *sid-1*, which is necessary for dsRNA transport into neurons (43-45). Enhanced neuronal RNAi can be obtained by ectopic neuronal expression of *sid-1* (46). Neuronal inactivation of *hpk-1* (*sid-1(pk3321); unc-119p::sid-1; unc-54p::Q35::YFP; hpk-1(RNAi)*) was sufficient to hasten the collapse of proteostasis within muscle cells, significantly increasing the number of polyQ aggregates (45 ± 1 vs 32 ± 1.1 at day 4) and paralysis rate (84% ± 0.04 vs 14% ± 0.04 at day 9) (Fig. 2A*iii*,D,E). Thus, HPK-1 functions within the nervous system regulates proteostasis in distal muscle tissue, which implies that HPK-1 coordinates organismal health through cell non-autonomous mechanisms.

To identify the signaling mechanism employed by HPK-1 to regulate distal proteostasis, we tested whether mutant animals impaired for neuropeptide and neurotransmitter transmission are essential for cell non-autonomous regulation of proteostasis (*unc-31* and *unc-13* mutants, respectively Fig. 2F). Neuronal expression of *hpk-1* in *unc-31* mutants improved proteostasis in the absence of neuropeptide transmission (Fig. 2G). In contrast, in the absence of neurotransmitter function, neuronal expression of *hpk-1* in *unc-13* mutants failed to improve proteostasis in muscle tissue (Fig. 2H). Thus, HPK-1 neuronal cell non-autonomous signaling occurs through neurotransmitter transmission.

Neuronal HPK-1 induces molecular chaperones and autophagy in distal tissues.

We sought to identify the components of the PN that are cell non-autonomously regulated via HPK-1 activity in the nervous system. We first tested whether neuronal HPK-1 overexpression alters the expression of molecular chaperones (*hsp-16.2p::GFP*) and found basal expression of molecular chaperones was unchanged (Supplementary Fig. 1A). In contrast, after heat shock, neuronal *hpk-1* overexpression increased *hsp-16.2p::GFP* expression, particularly in the pharynx and head muscles, but surprisingly not in intestinal cells (Fig. 3A,B, Supplementary Fig. 1B,C). We conclude that while *hpk-1* is required for the broad induction of molecular chaperones, neuronal HPK-1 primes inducibility of the heat shock response (HSR) within specific tissues, rather than in a systemic manner throughout the organism.

We next tested whether increased neuronal HPK-1 activity is sufficient to induce autophagy. Using an LGG-1/Atg8 fluorescent reporter strain to visualize autophagosome levels in hypodermal seam cells (*lgg-1p::LGG-1::GFP)* (47), we found that neuronal *hpk-1* overexpression significantly induces autophagy (Fig. 3C,D), but not in the intestine (Supplementary Fig. 1D,E). Thus, increased HPK-1 activity within the nervous system acts to induce autophagy cell non-autonomously within a subset of peripheral tissues.

Serotonergic and GABAergic HPK-1 differentially regulates heat stress response and autophagy.

To begin to identify the specific neuronal cell-types from which neuronal HPK-1 initiates distinct cell non-autonomous signals, we overexpressed *hpk-1* in different subtypes of neurons and assessed changes in muscle proteostasis (*unc-54p::Q35::YFP*). *hpk-1* overexpression in glutamatergic and dopaminergic neurons was not sufficient to decrease the formation of fluorescent foci or reduce paralysis (Supplementary Fig. 2). In contrast, overexpression of *hpk-1* in either serotonergic (*tph-1p::hpk-1*) or GABAergic (*unc-47p::hpk-1*) neurons was sufficient to improve proteostasis in muscle tissue and reduce paralysis (Fig. 4A-D). Accordingly, we found that *hpk-1* is

expressed in serotonergic and GABAergic neurons, based on colocalization between *hpk-1* and neuronal cell-type specific reporters (Fig. 4E,F, Supplementary Fig. 3), which suggests that HPK-1 initiates pro-longevity signals from these neurons to preserve muscle proteostasis.

We sought to determine whether signals initiated from serotonergic and GABAergic neurons induced similar or distinct components of the PN in distal tissues, and assess the overall consequence on organismal health. Since pan-neuronal expression of HPK-1 was sufficient to induce autophagy, improve thermotolerance, and increase lifespan, we chose to focus on these three phenotypes. Increased HPK-1 serotonergic signaling was sufficient to improve thermotolerance, without altering autophagy or lifespan (Fig. 5A-C, Supplementary Fig. 4A,B). In contrast, increased HPK-1 expression in GABAergic neurons did not alter thermotolerance, but induced autophagy and slightly but significantly increased lifespan (Fig. D-F, Supplementary Fig. 4C,D).

We sought to identify the mechanism through which increased neuronal HPK-1 activity induces autophagy in distal tissues. As expected loss of *tph-1,* which encodes the ortholog of human tryptophan hydroxylase 1 and is essential for the biosynthesis of serotonin (48), failed to block the induction of autophagy by increased neuronal *hpk-1* activity (Fig. 5G, *tph-1(mg280);rab-3p::hpk-1*). *unc-30* encodes the ortholog of human paired like homeodomain 2 (PITX2) and is essential for the proper differentiation of type-D inhibitory GABAergic motor neurons (49, 50). Loss of *unc-30* was sufficient to completely abrogate the induction of autophagy in seam cells after pan-neuronal overexpression of HPK-1 (Fig. 5G, *unc-30(ok613);rab-3p::hpk-1*). Collectively, we conclude that HPK-1 initiates distinct signals from serotonergic and GABAergic neurons to improve organismal health. Specifically, HPK-1 initiates serotonergic signals to improve survival to acute thermal stress, likely as a part of the HSF-1 thermosensory circuit (discussed below), and regulates GABAergic signals to increase lifespan through autophagy in the absence of stress (Fig. 6).

Discussion

In this study we show that HPK-1 expression in serotonergic neurons activates a cell non-autonomous signal to induce heat stress response and protein folding in muscles, whereas HPK-1 expression in GABAergic neurons signals the induction of autophagy activity in hypodermal tissue. A growing number of studies have demonstrated the nervous system plays a pivotable role in the regulation of overall organismal health and longevity. In response to metabolic, environmental, and intrinsic cues, the *C. elegans* nervous system can initiate a number of distinct stress and longevity signals cell non-autonomously, which activates comparable changes in gene expression peripheral tissues (15, 16, 18, 19, 51-55). We demonstrate a neuronal cell-type specific role for serotoninergic and GABAergic cell non-autonomous regulation of the PN by HPK-1. Loss of serotonin production in *tph-1* mutant animals has a minimal impact on lifespan at basal temperature (56). However, serotonin signaling is required for several conditions that extend longevity. For instance, animals treated with an atypical antidepressant serotonin antagonist (mianserin) (57), changes in food perception (58), and neuronal cell non-autonomous induction of the mitochondrial unfolded protein response (59, 60), all require *tph-1* and serotonin signaling. Furthermore, loss of the serotonin receptor *ser-1* is sufficient to increase lifespan (56). This is consistent with the notion that serotonergic neurons integrate diverse signals from sensory neurons to regulate gene expression in peripheral tissues that influence organismal longevity.

Surprisingly, we find that increased HPK-1 activity in serotonergic neurons does not increase lifespan, but is sufficient to improve muscle proteostasis and amplify the expression of molecular chaperones that maintain proteostasis within the cytosol and nucleus. Previous findings have discovered that ADF serotoninergic neurons receive upstream stress signals from the thermosensory circuit, consisting of the amphid sensory neurons (AFD) and the AIY interneurons, which regulate HSF-1 activity in the germline in a serotonin-dependent manner (16). Serotonin signaling and the serotonin receptor *ser-1* are essential for the induction of the HSR (15, 16). Interestingly, our results are analogous with a previous finding that demonstrated HSF-1 regulation of the HSR through thermosensory circuits is separable from lifespan (19). HPK-1 co-localizes with HSF-1 in neurons and is also essential for induction of the HSR (19, 23). Collectively, our results

suggest that HPK-1 is an integral part of the thermosensory-serotonin circuit to maintain homeostasis in response to acute thermal stress.

Increased HPK-1 activity in GABAergic neurons induces autophagy in peripheral cells, improves proteostasis and longevity. Whether HPK-1 functions in GABAergic neurons through alteration of GABA or another neurotransmitter is unknown, but proper differentiation of GABAergic neurons is essential for neuronal HPK-1 activation of autophagy in distal tissue. We posit HPK-1 cell non-autonomous signaling occurs via antagonism of GABA signaling. Loss of GABA increases *C. elegans* lifespan (61, 62). Interestingly, in mice GABA signaling inhibits autophagy and causes oxidative stress, which is mitigated via Tor1 inhibition (63). In fact, neuronal expression of HPK-1 is inhibited by TORC1 and *hpk-1* is essential for TORC1 inactivation to extend longevity and induce autophagy gene expression (23). Of note, TORC1 acts within neurons to regulate aging (64). Collectively, our results position HPK-1 activity in GABAergic neurons as the likely integration point for cell non-autonomous regulation of autophagy via TORC1.

This work reveals a new level of specificity in the capacity of the nervous system to initiate adaptive responses by triggering distinct components of the proteostatic network across cell types. Elucidating how neuronal cell-types generate heterotypic signals to coordinate the maintenance of homeostasis are just beginning to emerge. For example, a previous study discovered that activating non-autonomous signaling of the endoplasmic reticulum unfolded protein response (ER-UPR) via the XBP-1 transcription factor can be initiated from serotonergic neurons and dopaminergic neurons; these signals are unique and converge to activate distinct branches of the ER-UPR within intestinal cells (65). In contrast, our work demonstrates differential, yet specific, activation of cytosolic components of the PN in separate peripheral tissues. Our work suggests an emerging biological principle for the cell non-autonomous regulation of longevity: the nervous system partitions neuronal cell-types to coordinate the activation of complementary proteostatic mechanisms throughout tissues, despite utilizing the same transcriptional regulator within each neuronal cell-type. This is consistent with recent findings: during development and differentiation,

transcriptional rewiring of cells set chaperoning capacities and alter usage of mechanisms that maintain protein quality control (66, 67). Our work has revealed a novel insight into how an emerging transcriptional circuit within the nervous system of metazoans integrates diverse stimuli to coordinate specific adaptive responses to determine organismal aging.

Materials and Methods

C. elegans strains and details

All strains were maintained at 20°C on standard NGM plates with OP50. For all experiments, animals were grown in 20x concentrated HT115 bacteria seeded on 6cm RNAi plates. Details on the strains, mutant alleles, and transgenic animals used in this study are listed in Supplemental Table 1.

Generation of transgenic strains

To assemble tissue-specific constructs for overexpression experiments, the *hpk-1* cDNA was cloned under control of the following promoters: hypodermal *dpy-7p (68)*, body wall muscle *myo-3p (69)*, pan-neuronal *rab-3p* (70), dopaminergic neurons *cat-2p (71)*, glutamatergic neurons *eat-4p (72)*, serotonergic neurons *tph-1p (48)*, and g-aminobutyric acid (GABA)ergic neurons *unc-47p (73)*. All plasmids contained the *unc-54* 3'-UTR. These constructs for were injected at 5 ng/ml together with *myo-2p::mCherry* construct at 5 ng/ml as injection marker.

RNAi feeding

The *hpk-1* RNAi clone was originated from early copies of *E. coli* glycerol stocks of the comprehensive RNAi librariy generated in the Ahringer laboratory. The control empty vector (L4440) and *hpk-1* RNAi colonies were grown overnight in Luria broth with 50 µg ml–1 ampicillin and then seeded onto 6cm RNAi agar plates containing 5 mM isopropylthiogalactoside (IPTG) to induce dsRNA expression overnight at room temperature. RNAi clones used in this study were verified by DNA sequencing and subsequent BLAST analysis to confirm their identity.

The transmembrane protein *sid-1* is essential for dsRNA transport into the cell (43-45), however, *C. elegans* nervous system does not express *sid-1.* Enhanced neuronal RNAi can be obtained by ectopic neuronal expression of *sid-1* (46). Thus, we crossed the *rgef-1p::Q40::YFP* reporter with *sid-1(pk3321);unc-119p::sid*-1 for neuronal downregulation experiments.

Lifespan analysis

Lifespan assays were performed essentially as described in: (23, 74). Briefly, animals were synchronized by egg prep bleaching followed by hatching in M9 solution at 20°C overnight. The L1 animals were seeded onto 6cm plates with HT115 bacteria and allowed to develop at 20°C. At L4 stage, 2' fluoro– 5'deoxyuridine (FUDR) was added to a final concentration of 400 uM to prevent progeny production (defined as day 0 adulthood). Viability was scored every day or every other day as indicated in each figure. Prism 7 was used to for statistical analyses and the *P* values were calculated using log-rank (Mantel-Cox) method.

Thermotolerance assay

Survival assays at high temperature were conducted as previously described in (75). In brief, synchronized L1 animals were allowed to develop at 20°C; FUDR was added at the L4 stage to prevent progeny production. At day 1 adulthood, animals were moved to 35°C for a period of 6 and 8 hours. Animals were allowed to recover for 2 hours at 20°C, and viability was scored. Statistical testing between pairs of conditions for differences in the number of foci was performed using student's *t* test analysis.

Induction of *hsp-16.2p*::*GFP* after heat shock

The *hsp-16.2p*::*GFP* animals were heat shocked on day 1 of adulthood for 1 hour at 35°C and imaged after 4 hours of recovery. Images were acquired using a Zeiss Axio Imager M2m microscope with AxioVision v4.8.2.0 software. The GFP a.u. values from the head and intestine of

the animals were acquired using the area selection feature from AxioVision software. Two independent trials with a minimum of 20 animals per experiment were performed.

Measurement of autophagosome formation using the *GFP::LGG-1/Atg8* reporter.

GFP::LGG-1/Atg8 foci formation was visualized as described in (47). Briefly, L4 stage and day 1 adult animals were raised on HT115 bacteria at 20°C and imaged using a Zeiss Axio Imager M2m microscope with AxioVision v4.8.2.0 software at 63X magnification. More than 40 seam cells from 15-20 different animals were scored for *GFP::LGG-1* puncta accumulation. Two independent trials with a minimum of 20 animals per experiment were performed.

Polyglutamine aggregation in muscle and paralysis analyses

The visualization and quantification of the progressive decline in proteostasis in muscle tissue was performed as described in (42, 76). Briefly, synchronized *unc-54p*::*polyQ35*::*YFP* L4 animals were treated with FUDR to prevent progeny production. Then, fluorescent foci from 20 animals per technical replicate were scored blind daily from days one to three of adulthood. To assess paralysis, at days 5,7,9 and 11 of adulthood, prodded animals that responded with head movement (and were therefore still alive) but no backward or repulsive motion were scored as paralyzed (as described in (76)). Statistical testing between pairs of conditions for differences in the number of foci was performed using student's *t* test analysis. Two to five independent transgenics lines were tested.

Statistical analyses

Graphpad PRISM7 software was used for all statistical analyses. Data were considered statistically significant when *P* value was lower than 0.05. In figures, asterisks denote statistical significance as (*, $P < 0.05$, **, $P < 0.001$, ****, $P < 0.0001$) as compared to appropriate controls. N number listed in figure legend indicates the number of one representative experiment among all biological trials.

Data availability

All data supporting the findings of this study are available within the article, its Supplementary Information files, the peer-review file, or are available upon request.

Acknowledgments

We would like to thank members of the Samuelson laboratory, past and present, for their thoughtful insight in many discussions related to this project. In this regard, we would particularly like to thank Adam Cornwell. We would like to thank members of the Western New York Worm Group for their input and discussions. We would like to thank Dr. Doug Portman (URMC) and his laboratory for strains and advice. Some strains were provided by the CGC, which is funded by NIH Office of Research Infrastructure Programs (P40 OD010440). We would like to personally thank Dr. Dirk Bohmann (URMC) for the critical reading of this manuscript. Research reported in this publication was supported by the National Institute On Aging of the National Institutes of Health under Award Number RF1AG062593. CADB was supported by F32HD105323. The content is solely the responsibility of the authors and does not necessarily represent the official views of the National Institutes of Health.

References

1. Kikis EA, Gidalevitz T, & Morimoto RI (2010) Protein homeostasis in models of aging and age-related conformational disease. *Advances in experimental medicine and biology* 694:138-159.
2. Taylor RC & Dillin A (2011) Aging as an event of proteostasis collapse. *Cold Spring Harbor perspectives in biology* 3(5).
3. Balch WE, Morimoto RI, Dillin A, & Kelly JW (2008) Adapting proteostasis for disease intervention. *Science* 319(5865):916-919.
4. Gidalevitz T, Ben-Zvi A, Ho KH, Brignull HR, & Morimoto RI (2006) Progressive disruption of cellular protein folding in models of polyglutamine diseases. *Science* 311(5766):1471-1474.
5. Gidalevitz T, Kikis EA, & Morimoto RI (2010) A cellular perspective on conformational disease: the role of genetic background and proteostasis networks. *Curr Opin Struct Biol* 20(1):23-32.
6. Sala AJ, Bott LC, & Morimoto RI (2017) Shaping proteostasis at the cellular, tissue, and organismal level. *J Cell Biol* 216(5):1231-1241.
7. Morimoto RI (2011) The heat shock response: systems biology of proteotoxic stress in aging and disease. *Cold Spring Harb Symp Quant Biol* 76:91-99.
8. Morimoto RI (2019) Cell-Nonautonomous Regulation of Proteostasis in Aging and Disease. *Cold Spring Harbor perspectives in biology*.
9. Jaisson S & Gillery P (2014) Impaired proteostasis: role in the pathogenesis of diabetes mellitus. *Diabetologia* 57(8):1517-1527.
10. Lopez-Otin C, Blasco MA, Partridge L, Serrano M, & Kroemer G (2013) The hallmarks of aging. *Cell* 153(6):1194-1217.
11. Labbadia J & Morimoto RI (2015) The biology of proteostasis in aging and disease. *Annu Rev Biochem* 84:435-464.
12. Lazaro-Pena MI*, et al.* (2022) HSF-1: Guardian of the Proteome Through Integration of Longevity Signals to the Proteostatic Network. *Frontiers in Aging* 3.
13. Hildegard IDM, Thomas H, & Coleen TM (2018) The nematode Caenorhabditis elegans as a model for aging research. *Drug Discovery Today: Disease Models* 27:3-13.
14. Miller HA, Dean ES, Pletcher SD, & Leiser SF (2020) Cell non-autonomous regulation of health and longevity. *Elife* 9.
15. Prahlad V, Cornelius T, & Morimoto RI (2008) Regulation of the cellular heat shock response in Caenorhabditis elegans by thermosensory neurons. *Science* 320(5877):811-814.
16. Tatum MC*, et al.* (2015) Neuronal serotonin release triggers the heat shock response in C. elegans in the absence of temperature increase. *Curr Biol* 25(2):163-174.
17. Garcia SM, Casanueva MO, Silva MC, Amaral MD, & Morimoto RI (2007) Neuronal signaling modulates protein homeostasis in Caenorhabditis elegans post-synaptic muscle cells. *Genes Dev* 21(22):3006-3016.

18. Silva MC, Amaral MD, & Morimoto RI (2013) Neuronal reprograming of protein homeostasis by calcium-dependent regulation of the heat shock response. *PLoS Genet* 9(8):e1003711.
19. Douglas PM*, et al.* (2015) Heterotypic Signals from Neural HSF-1 Separate Thermotolerance from Longevity. *Cell Rep* 12(7):1196-1204.
20. Kumsta C*, et al.* (2014) Integrin-linked kinase modulates longevity and thermotolerance in C. elegans through neuronal control of HSF-1. *Aging Cell* 13(3):419-430.
21. Samuelson AV, Carr CE, & Ruvkun G (2007) Gene activities that mediate increased life span of C. elegans insulin-like signaling mutants. *Genes Dev* 21(22):2976-2994.
22. Berber S*, et al.* (2016) Homeodomain-Interacting Protein Kinase (HPK-1) regulates stress responses and ageing in C. elegans. *Scientific reports* 6:19582.
23. Das R*, et al.* (2017) The homeodomain-interacting protein kinase HPK-1 preserves protein homeostasis and longevity through master regulatory control of the HSF-1 chaperone network and TORC1-restricted autophagy in Caenorhabditis elegans. *PLoS Genet* 13(10):e1007038.
24. Hofmann TG, Stollberg N, Schmitz ML, & Will H (2003) HIPK2 regulates transforming growth factor-beta-induced c-Jun NH(2)-terminal kinase activation and apoptosis in human hepatoma cells. *Cancer Res* 63(23):8271-8277.
25. Kim EA*, et al.* (2006) Phosphorylation and transactivation of Pax6 by homeodomain-interacting protein kinase 2. *J Biol Chem* 281(11):7489-7497.
26. Lee P, Cho BR, Joo HS, & Hahn JS (2008) Yeast Yak1 kinase, a bridge between PKA and stress-responsive transcription factors, Hsf1 and Msn2/Msn4. *Mol Microbiol* 70(4):882-895.
27. Shojima N*, et al.* (2012) Depletion of homeodomain-interacting protein kinase 3 impairs insulin secretion and glucose tolerance in mice. *Diabetologia* 55(12):3318-3330.
28. Calzado MA, Renner F, Roscic A, & Schmitz ML (2007) HIPK2: a versatile switchboard regulating the transcription machinery and cell death. *Cell Cycle* 6(2):139-143.
29. Rinaldo C, Siepi F, Prodosmo A, & Soddu S (2008) HIPKs: Jack of all trades in basic nuclear activities. *Biochim Biophys Acta* 1783(11):2124-2129.
30. de la Vega L*, et al.* (2012) A redox-regulated SUMO/acetylation switch of HIPK2 controls the survival threshold to oxidative stress. *Mol Cell* 46(4):472-483.
31. Song JJ & Lee YJ (2003) Effect of glucose concentration on activation of the ASK1-SEK1-JNK1 signal transduction pathway. *J Cell Biochem* 89(4):653-662.
32. Song JJ & Lee YJ (2003) Role of the ASK1-SEK1-JNK1-HIPK1 signal in Daxx trafficking and ASK1 oligomerization. *J Biol Chem* 278(47):47245-47252.
33. Ecsedy JA, Michaelson JS, & Leder P (2003) Homeodomain-interacting protein kinase 1 modulates Daxx localization, phosphorylation, and transcriptional activity. *Mol Cell Biol* 23(3):950-960.
34. Garufi A*, et al.* (2013) Glucose restriction induces cell death in parental but not in homeodomain-interacting protein kinase 2-depleted RKO colon cancer cells:

molecular mechanisms and implications for tumor therapy. *Cell death & disease* 4:e639.
35. Baldari S*, et al.* (2017) Hyperglycemia triggers HIPK2 protein degradation. *Oncotarget* 8(1):1190-1203.
36. Berber S*, et al.* (2013) Homeodomain interacting protein kinase (HPK-1) is required in the soma for robust germline proliferation in C. elegans. *Developmental dynamics : an official publication of the American Association of Anatomists* 242(11):1250-1261.
37. Hattangadi SM, Burke KA, & Lodish HF (2010) Homeodomain-interacting protein kinase 2 plays an important role in normal terminal erythroid differentiation. *Blood* 115(23):4853-4861.
38. Steinmetz EL, Dewald DN, & Walldorf U (2018) Homeodomain-interacting protein kinase phosphorylates the Drosophila Paired box protein 6 (Pax6) homologues Twin of eyeless and Eyeless. *Insect molecular biology* 27(2):198-211.
39. Rinaldo C, Prodosmo A, Siepi F, & Soddu S (2007) HIPK2: a multitalented partner for transcription factors in DNA damage response and development. *Biochemistry and cell biology = Biochimie et biologie cellulaire* 85(4):411-418.
40. Herndon LA*, et al.* (2002) Stochastic and genetic factors influence tissue-specific decline in ageing C. elegans. *Nature* 419(6909):808-814.
41. Huang C, Xiong C, & Kornfeld K (2004) Measurements of age-related changes of physiological processes that predict lifespan of Caenorhabditis elegans. *Proc Natl Acad Sci U S A* 101(21):8084-8089. Epub 2004 May 8012.
42. Morley JF, Brignull HR, Weyers JJ, & Morimoto RI (2002) The threshold for polyglutamine-expansion protein aggregation and cellular toxicity is dynamic and influenced by aging in Caenorhabditis elegans. *Proc Natl Acad Sci U S A* 99(16):10417-10422.
43. Timmons L, Court DL, & Fire A (2001) Ingestion of bacterially expressed dsRNAs can produce specific and potent genetic interference in Caenorhabditis elegans. *Gene* 263(1-2):103-112.
44. Winston WM, Molodowitch C, & Hunter CP (2002) Systemic RNAi in C. elegans requires the putative transmembrane protein SID-1. *Science* 295(5564):2456-2459.
45. Kamath RS*, et al.* (2003) Systematic functional analysis of the Caenorhabditis elegans genome using RNAi. *Nature* 421(6920):231-237.
46. Calixto A, Chelur D, Topalidou I, Chen X, & Chalfie M (2010) Enhanced neuronal RNAi in C. elegans using SID-1. *Nature methods* 7(7):554-559.
47. Kumsta C, Chang JT, Schmalz J, & Hansen M (2017) Hormetic heat stress and HSF-1 induce autophagy to improve survival and proteostasis in C. elegans. *Nature communications* 8:14337.
48. Sze JY, Victor M, Loer C, Shi Y, & Ruvkun G (2000) Food and metabolic signalling defects in a Caenorhabditis elegans serotonin-synthesis mutant. *Nature* 403(6769):560-564.
49. McIntire SL, Jorgensen E, & Horvitz HR (1993) Genes required for GABA function in Caenorhabditis elegans. *Nature* 364(6435):334-337.

50. Jin Y, Hoskins R, & Horvitz HR (1994) Control of type-D GABAergic neuron differentiation by C. elegans UNC-30 homeodomain protein. *Nature* 372(6508):780-783.
51. Durieux J, Wolff S, & Dillin A (2011) The cell-non-autonomous nature of electron transport chain-mediated longevity. *Cell* 144(1):79-91.
52. Taylor RC & Dillin A (2013) XBP-1 is a cell-nonautonomous regulator of stress resistance and longevity. *Cell* 153(7):1435-1447.
53. Prahlad V & Morimoto RI (2011) Neuronal circuitry regulates the response of Caenorhabditis elegans to misfolded proteins. *Proc Natl Acad Sci U S A* 108(34):14204-14209.
54. Imanikia S, Ozbey NP, Krueger C, Casanueva MO, & Taylor RC (2019) Neuronal XBP-1 Activates Intestinal Lysosomes to Improve Proteostasis in C. elegans. *Curr Biol* 29(14):2322-2338 e2327.
55. Frakes AE*, et al.* (2020) Four glial cells regulate ER stress resistance and longevity via neuropeptide signaling in C. elegans. *Science* 367(6476):436-440.
56. Murakami H & Murakami S (2007) Serotonin receptors antagonistically modulate Caenorhabditis elegans longevity. *Aging Cell* 6(4):483-488.
57. Petrascheck M, Ye X, & Buck LB (2007) An antidepressant that extends lifespan in adult Caenorhabditis elegans. *Nature* 450(7169):553-556.
58. Entchev EV*, et al.* (2015) A gene-expression-based neural code for food abundance that modulates lifespan. *Elife* 4:e06259.
59. Zhang Q*, et al.* (2018) The Mitochondrial Unfolded Protein Response Is Mediated Cell-Non-autonomously by Retromer-Dependent Wnt Signaling. *Cell* 174(4):870-883 e817.
60. Berendzen KM*, et al.* (2016) Neuroendocrine Coordination of Mitochondrial Stress Signaling and Proteostasis. *Cell* 166(6):1553-1563 e1510.
61. Chun L*, et al.* (2015) Metabotropic GABA signalling modulates longevity in C. elegans. *Nature communications* 6:8828.
62. Yuan F*, et al.* (2019) GABA receptors differentially regulate life span and health span in C. elegans through distinct downstream mechanisms. *Am J Physiol Cell Physiol* 317(5):C953-C963.
63. Lakhani R*, et al.* (2014) Defects in GABA metabolism affect selective autophagy pathways and are alleviated by mTOR inhibition. *EMBO Mol Med* 6(4):551-566.
64. Zhang Y*, et al.* (2019) Neuronal TORC1 modulates longevity via AMPK and cell nonautonomous regulation of mitochondrial dynamics in C. elegans. *Elife* 8.
65. Higuchi-Sanabria R*, et al.* (2020) Divergent Nodes of Non-autonomous UPR(ER) Signaling through Serotonergic and Dopaminergic Neurons. *Cell Rep* 33(10):108489.
66. Shemesh N*, et al.* (2021) The landscape of molecular chaperones across human tissues reveals a layered architecture of core and variable chaperones. *Nature communications* 12(1):2180.
67. Nisaa K & Ben-Zvi A (2021) Chaperone networks are shaped by cellular differentiation and identity. *Trends Cell Biol*.

68. Gilleard JS, Barry JD, & Johnstone IL (1997) cis regulatory requirements for hypodermal cell-specific expression of the Caenorhabditis elegans cuticle collagen gene dpy-7. *Mol Cell Biol* 17(4):2301-2311.
69. Okkema PG, Harrison SW, Plunger V, Aryana A, & Fire A (1993) Sequence requirements for myosin gene expression and regulation in Caenorhabditis elegans. *Genetics* 135(2):385-404.
70. Nonet ML*, et al.* (1997) Caenorhabditis elegans rab-3 mutant synapses exhibit impaired function and are partially depleted of vesicles. *J Neurosci* 17(21):8061-8073.
71. Lints R & Emmons SW (1999) Patterning of dopaminergic neurotransmitter identity among Caenorhabditis elegans ray sensory neurons by a TGFbeta family signaling pathway and a Hox gene. *Development* 126(24):5819-5831.
72. Lee RY, Sawin ER, Chalfie M, Horvitz HR, & Avery L (1999) EAT-4, a homolog of a mammalian sodium-dependent inorganic phosphate cotransporter, is necessary for glutamatergic neurotransmission in caenorhabditis elegans. *J Neurosci* 19(1):159-167.
73. Gendrel M, Atlas EG, & Hobert O (2016) A cellular and regulatory map of the GABAergic nervous system of C. elegans. *Elife* 5.
74. Lee SS, Kennedy S, Tolonen AC, & Ruvkun G (2003) DAF-16 target genes that control C. elegans life-span and metabolism. *Science* 300(5619):644-647.
75. Johnson DW*, et al.* (2014) The Caenorhabditis elegans Myc-Mondo/Mad complexes integrate diverse longevity signals. *PLoS Genet* 10(4):e1004278.
76. Lazaro-Pena MI, Cornwell AB, & Samuelson AV (2021) Quantifying Tissue-Specific Proteostatic Decline in Caenorhabditis elegans. *Journal of visualized experiments : JoVE* (175).

Figures and Tables

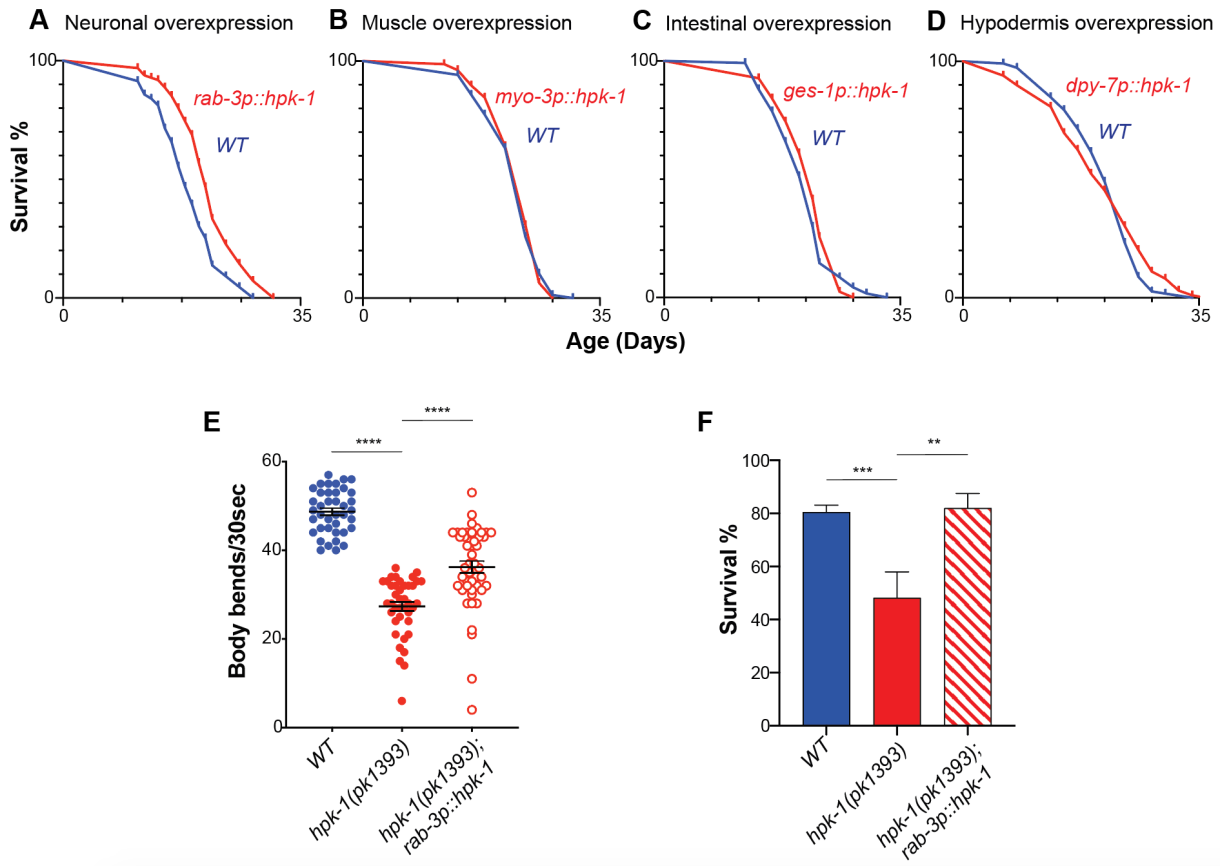

Figure 1. Neuronal HPK-1 extends longevity and promotes health span.

Survival curves of animals overexpressing *hpk-1* (red line) in the nervous system **(A)**, muscle **(B)**, intestine **(C)** and hypodermis **(D)** compared with control non-transgenic siblings (blue line). ($n \geq 175$, $P < 0.0001$ for A, $n \geq 78$ for B, $n \geq 82$ for C and $n \geq 105$ for D). Lifespan graphs are representative of two biological replicates. **(E)** Frequency of body bends of *wild type*, *rab-3p::hpk-1* and *hpk-1(pk1393); rab-3p::hpk-1* day 2 adult animals maintained ($n \geq 48$). **(F)** Survival of day 1 adult animals subjected to heat shock treatment. Graph represents one of the two individual trials ($n \geq 66$). See Supplemental Tables 2, 4 and 6 for details and additional trials.

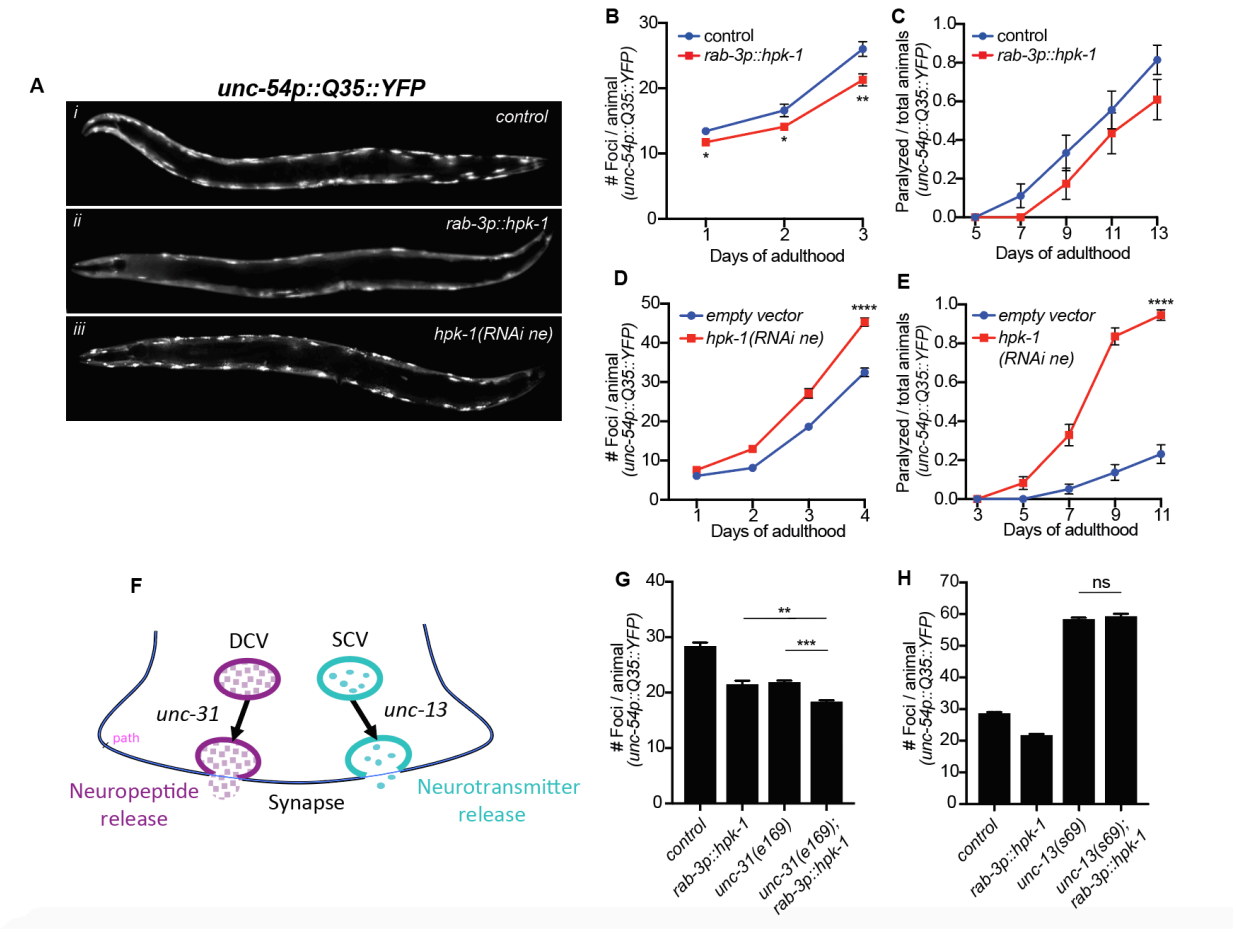

Figure 2. Neuronal HPK-1 prevents the decline in proteostasis through neurotransmitter release.

(A) Fluorescent micrographs of animals expressing the polyglutamine fluorescent reporter in muscle. (**B** and **C**) Quantification of foci in muscle (B) and paralysis rate (C). Graphs are representative of 5 individual transgenic lines (n≥18 for B and n≥23 for C). (**D** and **E**) Quantification of foci in muscle (D) and paralysis rate (E) in neuronal enhanced RNAi animals (n≥22 for D and n≥73 for E). **(F)** Neuropeptides and neurotransmitters are essential for neuronal signaling; vesicle release depends on *unc-31* and *unc-13*, respectively. (**G** and **H**) Quantification of foci in muscle (G) (n≥21), (H) (n≥21). *T* test analysis with $^{**}P < 0.01$ and $^{***}P < 0.001$. See Supplemental Tables 3 and 5 for details and additional trials.

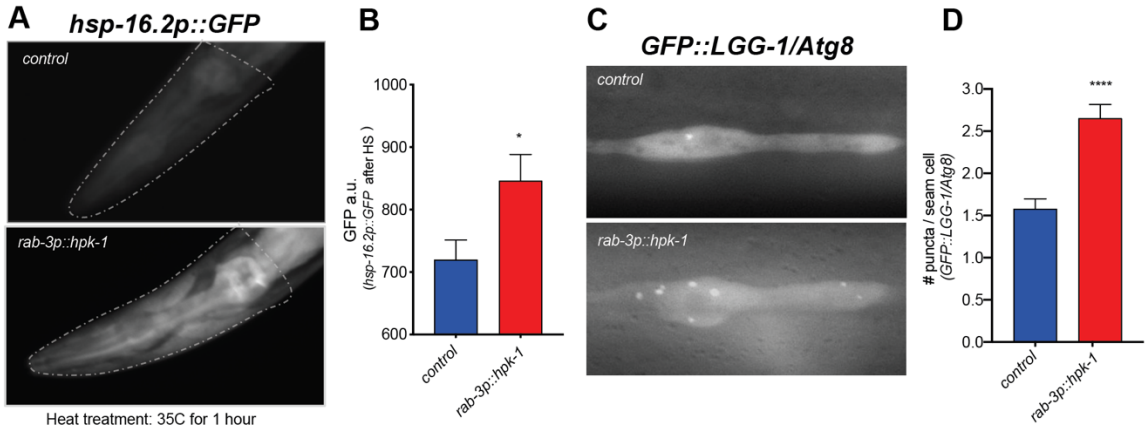

Figure 3. Neuronal HPK-1 induces the proteostatic network in distal tissues.

(A and **B)** Fluorescent micrographs (A) and fluorescent density quantification (B) of control and *rab-3p::hpk-1* of day 1 adult animals expressing *hsp-16.2::GFP* molecular chaperone reporter that were exposed to heat shock for 1 hour at 35°C ($n \geq 15$). **(C** and **D)** Fluorescent micrographs (C) and quantification (D) of puncta in seam cells of control and *rab-3p::hpk-1* of L4 stage animals expressing the *lgg-1p::GFP::LGG-1/Atg8* autophagosome reporter ($n \geq 43$). *T* test analysis with $^{*}P < 0.05$, $^{**}P < 0.01$, $^{***}P < 0.001$ and $^{****}P < 0.0001$. See Supplemental Tables 7 and 8 for details and additional trials.

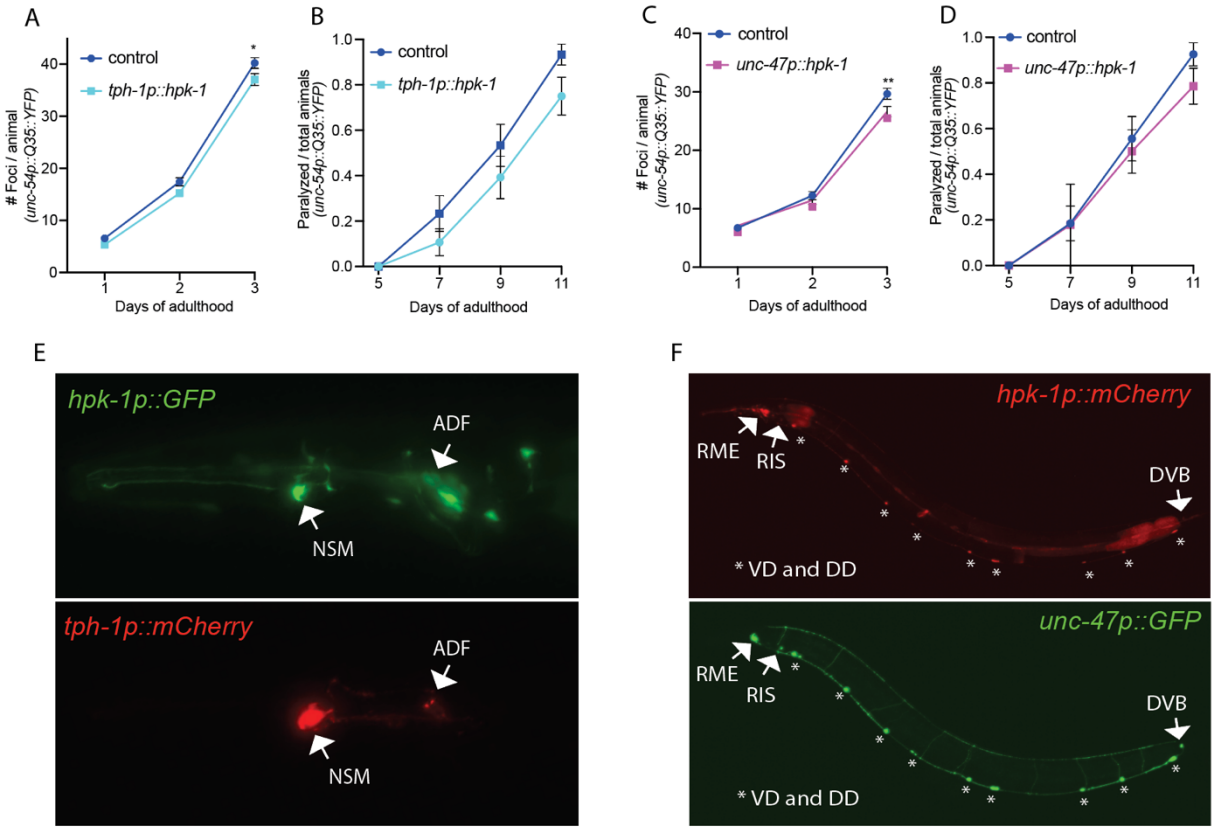

Figure 4. Expression of HPK-1 in serotonergic and GABAergic prevents the decline in proteostasis in muscle tissue.

(A and **B)** Quantification of foci (A) and paralysis rate (B) of animals expressing *hpk-1* in serotonergic neurons (n≥17 for A and n≥28 for B). **(C** and **D)** Quantification of foci (C) and paralysis rate (D) of animals expressing *hpk-1* in GABAergic neurons (n≥19 for C and n≥27 for D). **(E)** Fluorescent micrographs of endogenous *hpk-1* expression in serotonergic neurons. **(F)** Fluorescent micrographs of endogenous *hpk-1* expression in GABAergic neurons. See Supplemental Tables: 3 and 5 for details and additional trials.

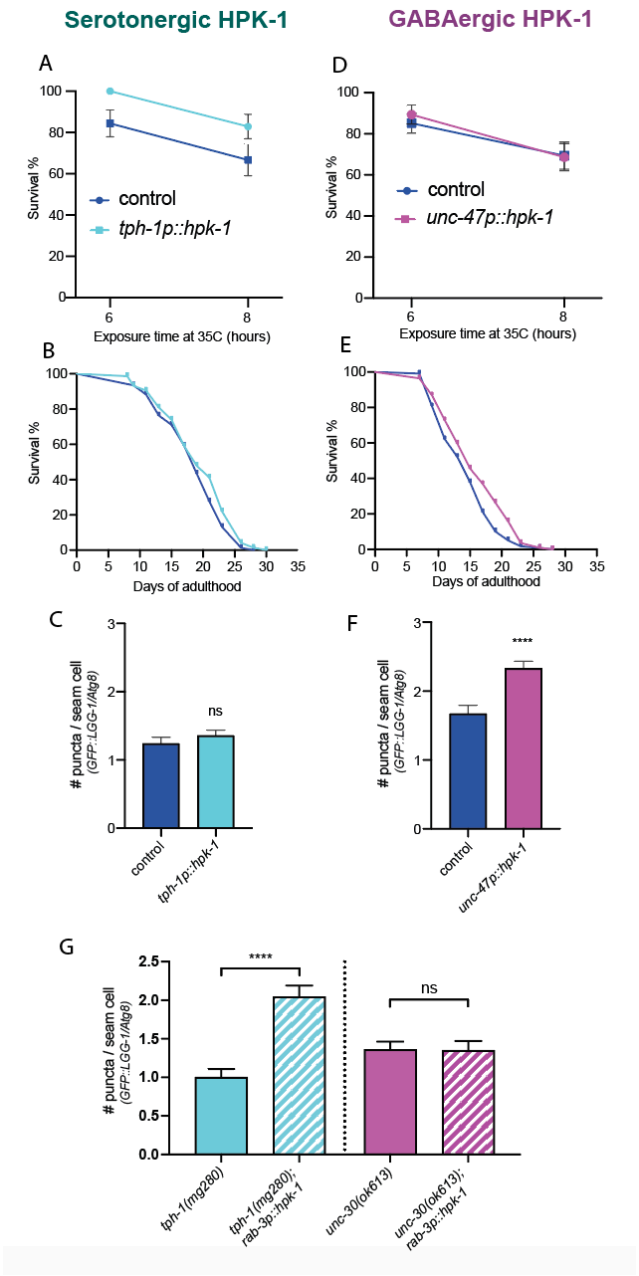

Figure 5. Serotonergic and GABAergic HPK-1 signaling activates distinct adaptive responses to regulate stress resistance and longevity.

(A) Survival of serotonergic HPK-1 day 1 adult animals after heat shock (n≥32). **(B)** Lifespan of serotonergic HPK-1 (n≥76). **(C)** Quantification of autophagosomes in hypodermal cells of

serotonergic HPK-1 day 1 adult animals (n≥80). **(D)** Survival of GABAergic HPK-1 day 1 adult animals after heat shock (n≥47). **(E)** Lifespan of GABAergic HPK-1 animals (n≥119). **(F)** Quantification of autophagosomes in hypodermal cells of GABAergic HPK-1 day 1 adult animals (n≥64). (**G**) Quantification of autophagosomes in hypodermal cells of mutant animals of serotonin and GABAergic signaling (*tph-1* and *unc-30*, respectively), expressing pan-neuronal HPK-1 (day 1 adults, n≥ 67). *T* test analysis with *$P < 0.05$, **$P < 0.01$ and ****$P < 0.0001$. See Supplemental Tables: 2, 6 and 8 for details and additional trials.

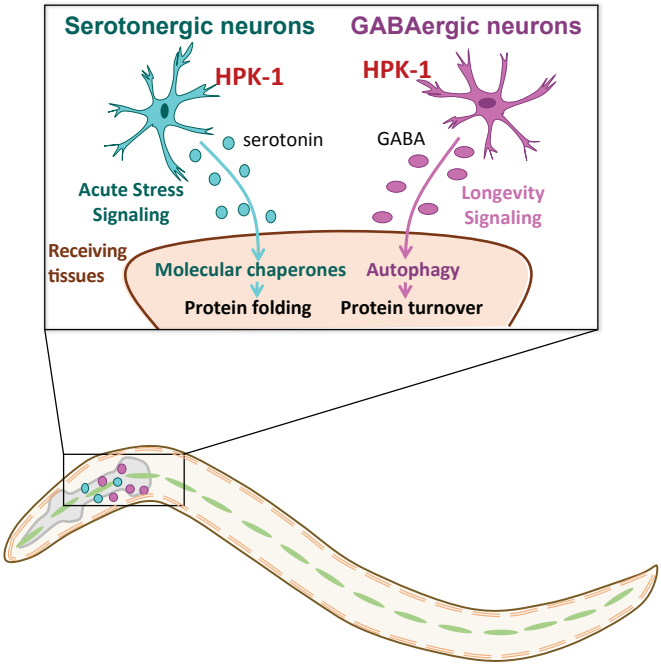

Figure 6. Model diagram of serotonergic and GABAergic HPK-1 regulatory mechanism to mediate proteostasis and longevity.

HPK-1 activity in serotonergic and GABAergic neurons initiates distinct adaptive responses, either of which improve proteostasis in a cell non-autonomous manner. Serotonergic HPK-1 protects the proteome from acute stress, while GABAergic HPK-1 fortifies the proteome by regulating autophagy activity in response to other types of stress, such as metabolic stress.

Supplementary Information

Title:
Neuroendocrine control of the proteostatic network by HPK-1 delays aging

Authors: Maria I. Lazaro-Pena[1], Carlos A. Diaz-Balzac[2], Ritika Das[1,3,4], Andrew Samuelson[1*]

Contains:

Supplementary figure and figure legends
Supplementary tables

Supplementary figures and figure legends:

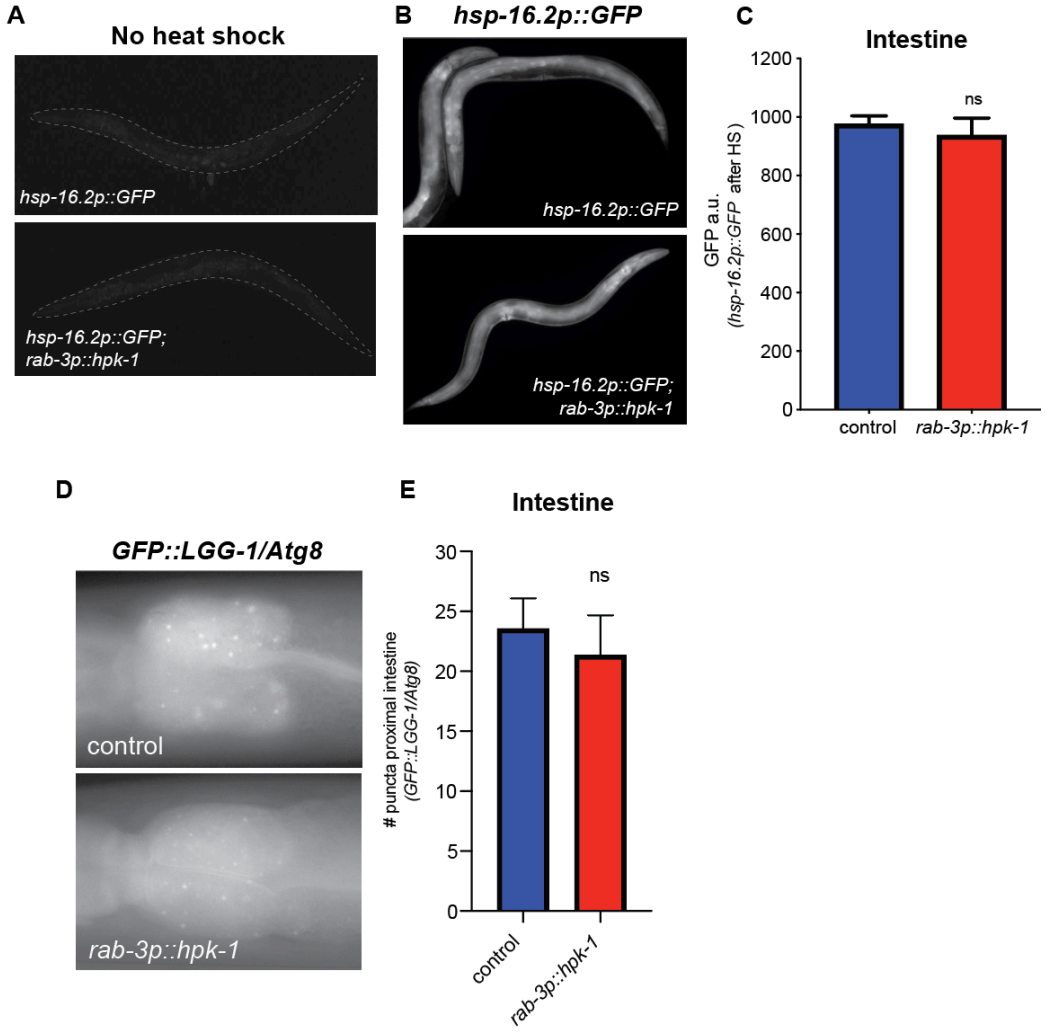

Figure S1. Neuronal HPK-1 does not hyper-induces molecular chaperones in the intestine. (A) Animals expressing *hsp-16.2p::GFP* in basal condition. **(B)** Animals expressing *hsp-16.2p::GFP* after heat shock treatment for 1hr at 35°C. **(C)** GFP densitometry quantification on the intestine of day 1 adults after heat treatment from *hsp-16.2p::GFP* expressing animals (n≥24). (D) Fluorescent micrographs and (E) quantification of puncta in proximal intestinal cells of control and *rab-3p::hpk-1* of L4 stage animals expressing the *lgg-1p::GFP::LGG-1/Atg8* autophagosome reporter (n≥17). See Supplemental Table 7 and 8 for details and additional trials.

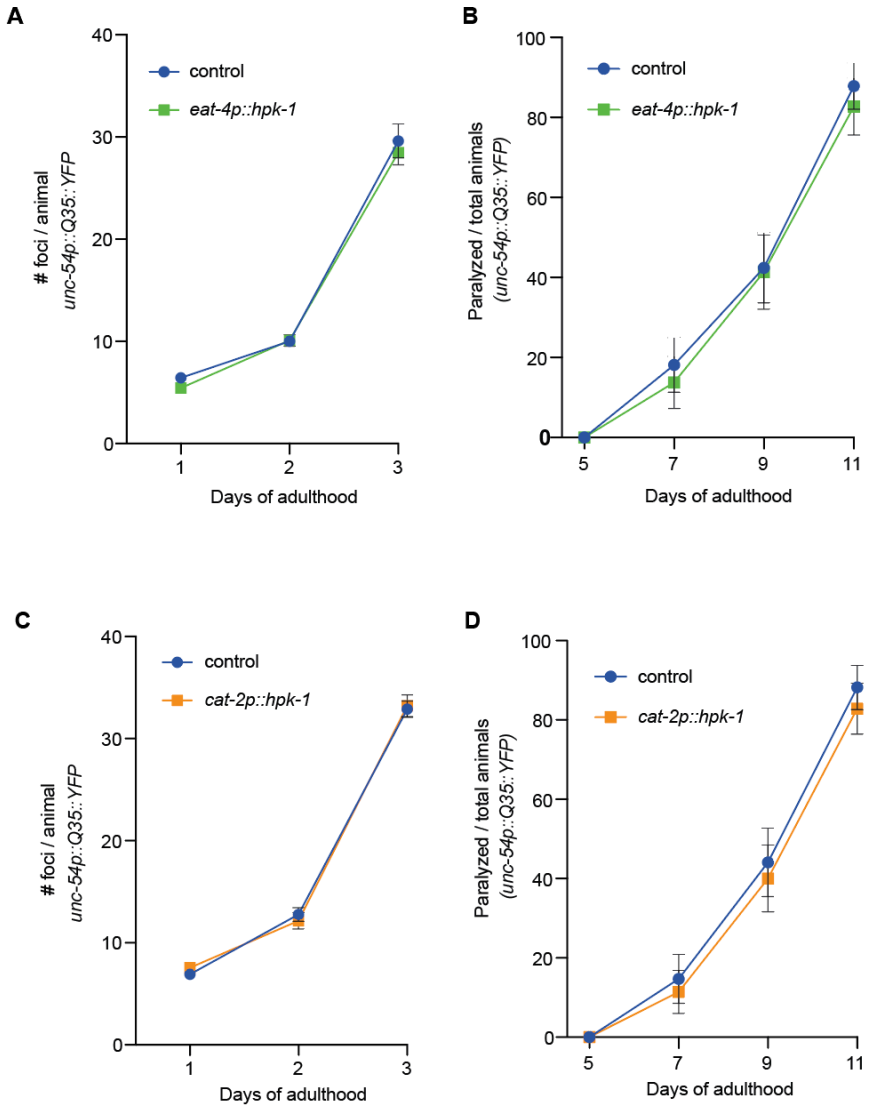

Figure S2. *hpk-1* expression in glutamatergic and dopaminergic neurons is not sufficient to prevent the decline in proteostasis. (A and **B)** Quantification of number of foci (A) and paralysis rate (B) of animals expressing *hpk-1* in the glutamatergic neurons (*eat-4p::hpk-1*; green line) and control non-transgenic siblings (blue line) ($n \geq 18$ for A and $n \geq 29$ for B). **(C** and **D)** Quantification of number of foci (C) and paralysis rate (D) of animals expressing *hpk-1* in the dopaminergic neurons (*cat-2p::hpk-1;* orange line) and control non-transgenic siblings (blue line) ($n \geq 16$ for C and $n \geq 34$ for D). See Supplemental Tables 3 and 5 for details and additional trials.

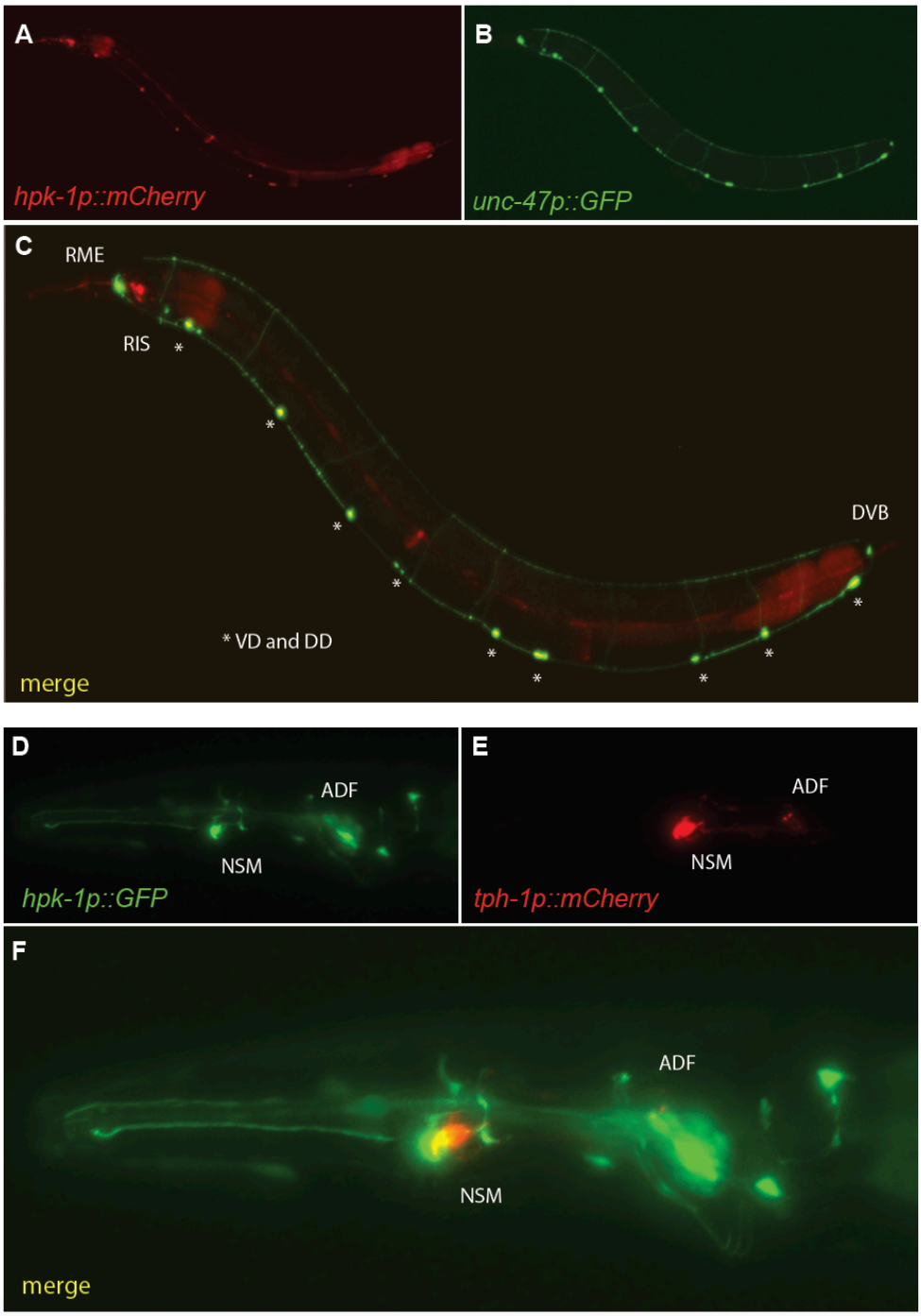

Figure S3. *hpk-1* is expressed in GABAergic and serotonergic neurons. Representative fluorescent micrographs of day 1 adult animals co-expressing *hpk-1p::mCherry* and *unc-47p::GFP* **(A-C)**; and *hpk-1p::GFP* and *tph-1p::mCherry* **(D-F)**.

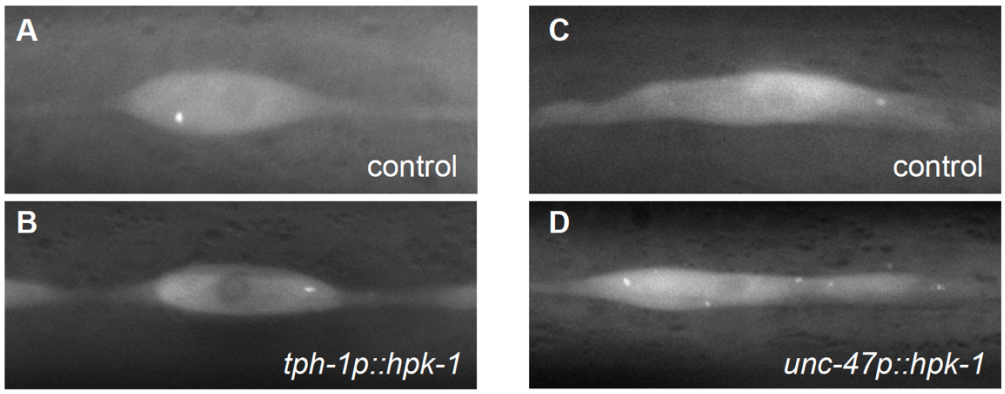

Figure S4. *hpk-1* expression in GABAergic neurons, but not in serotonergic neurons, induces autophagy activity in hypodermal seam cells. Representative fluorescent micrographs (from data in Figure 5I,K), showing autophagosome fluorescent puncta in seam cells of day 1 adult animals expressing *GFP::LGG-1/Atg8* autophagosome reporter with *hpk-1* expression in serotonergic (**A** and **B**) and GABAergic (**C** and **D**) neurons.

Supplementary tables:

Table S1. Strains, mutant alleles, and transgenic animals used in this study.

Strain name	Genotype
N2	*Wild type*
AVS392	*hpk-1(pk1393) X*
AVS543	*artEx41 [rab-3p::hpk-1::CFP + pCFJ90 (myo-2p::mCherry)]*
AVS609	*artEx43 [myo-3p::hpk-1 + pCFJ90 (myo-2p::mCherry)] line 1*
AVS614	*artEx48 [dpy-7p::hpk-1 + pCFJ90 (myo-2p::mCherry)] line 1*
AVS627	*artEx52 [ges-1p::hpk-1 + pCFJ90 (myo-2p::mCherry)] line 1*
AVS420	*hpk-1(pk1393) X; artEx41 [rab-3p::hpk-1::CFP + pCFJ90 (myo-2p::mCherry)]*
AVS832	*rmIs132 [unc-54p::Q35::YFP] I; artEx58 [rab-3p::hpk-1 + pCFJ90 (myo-2p::mCherry)] line 1*
AVS833	*rmIs132 [unc-54p::Q35::YFP] I; artEx59 [rab-3p::hpk-1 + pCFJ90 (myo-2p::mCherry)] line 2*
AVS834	*rmIs132 [unc-54p::Q35::YFP] I; artEx60 [rab-3p::hpk-1 + pCFJ90 (myo-2p::mCherry)] line 3*
AVS835	*rmIs132 [unc-54p::Q35::YFP] I; artEx61 [rab-3p::hpk-1 + pCFJ90 (myo-2p::mCherry)] line 4*
AVS562	*rmIs132 [unc-54p::Q35::YFP] I; artEx41 [rab-3p::hpk-1::CFP + pCFJ90 (myo-2p::mCherry)] line 5*
AVS214/HC196	*sid-1(qt9) V*
AVS265/TU3401	*sid-1(pk3321)V; uIs69 [unc-119p::sid-1; myo-2p::mCherry]V*
AVS540	*rmIs132 [unc-54p::Q35::YFP] I; sid-1(pk3321)V; uIs69[unc-119p::sid-1; myo-2p::mCherry]V*
AVS713	*rmIs132 [unc-54p::Q35::YFP] I; artEx41(rab-3p::hpk-1::CFP + pCFJ90 (myo-2p::mCherry)]; unc-31(e169)V*
AVS810	*rmIs132 [unc-54p::Q35::YFP] I; artEx41 [rab-3p::hpk-1::CFP + pCFJ90 (myo-2p::mCherry)]; unc-13(e51)I*
AVS84/TJ375	*gpIs1 [hsp-16.2p::GFP] IV*
AVS397	*gpIs1 [hsp-16.2p::GFP]; artEx35 [sur-5p::hpk-1::CFP +pCFJ90 (myo-2p::mCherry)]*
AVS399	*gpIs1 [hsp-16.2p::GFP]; artEx33 [rab-3p::hpk-1::CFP +pCFJ90 (myo-2p::mCherry)]*
AVS716	*artEx41 [rab-3p::hpk-1::CFP + pCFJ90 (myo-2p::mCherry)]; sqIs13 [lgg-1p::GFP::lgg-1 + odr-1p::RFP]*
AVS682	*artEx62 [tph-1p::hpk-1 + pCFJ90 (myo-2p::mCherry)] line 1; rmIs132 [unc-54p::Q35::YFP] I*
AVS683	*artEx63 [tph-1p::hpk-1 + pCFJ90 (myo-2p::mCherry)] line 2; rmIs132 [unc-54p::Q35::YFP] I*
AVS685	*artEx65 [unc-47p::hpk-1 + pCFJ90 (myo-2p::mCherry)] line 1; rmIs132 [unc-54p::Q35::YFP] I*
AVS686	*artEx66 [unc-47p::hpk-1 + pCFJ90 (myo-2p::mCherry)] line 2; rmIs132 [unc-54p::Q35::YFP] I*
AVS691	*artEx71 [eat-4p::hpk-1 + pCFJ90 (myo-2p::mCherry)] line 1; rmIs132 [unc-54p::Q35::YFP] I*
AVS692	*artEx72 [eat-4p::hpk-1 + pCFJ90 (myo-2p::mCherry)] line 2; rmIs132 [unc-54p::Q35::YFP] I*
AVS693	*artEx73 [cat-2p::hpk-1 + pCFJ90 (myo-2p::mCherry)] line 1; rmIs132 [unc-54p::Q35::YFP] I*
AVS694	*artEx74 [cat-2p::hpk-1 + pCFJ90 (myo-2p::mCherry)] line 2; rmIs132 [unc-54p::Q35::YFP] I*
AVS809	*artEx62 [tph-1p::hpk-1 + pCFJ90 (myo-2p::mCherry)] line 1; sqIs13 [lgg-1p::GFP::lgg-1 + odr-1p::RFP]*
AVS794	*artEx65 [unc-47p::hpk-1 + pCFJ90 (myo-2p::mCherry)] line 1; sqIs13 [lgg-1p::GFP::lgg-1 + odr-1p::RFP]*
AVS709	*artEx62 [tph-1p::hpk-1 + pCFJ90 (myo-2p::mCherry)] line 1*
AVS710	*artEx65 [unc-47p::hpk-1 + pCFJ90 (myo-2p::mCherry)] line 1*
AVS836	*artEx91 [hpk-1p::GFP + tph-1p::mCherry] line 1*
AVS757	artEx87 [hpk-1p::mCherry + unc-47p::GFP] line 1
AVS816	*artEx41(rab-3p::hpk-1::CFP + pCFJ90 (myo-2p::mCherry); sqIs24 [lgg-1p::GFP::lgg-1 + unc-122p::RFP]; unc-30(ok613)*
AVS872	*artEx41(rab-3p::hpk-1::CFP + pCFJ90 (myo-2p::mCherry); sqIs24 [lgg-1p::GFP::lgg-1 + unc-122p::RFP]; tph-1(mg280)*

Strains with both an AVS# and an external designation were generated in another laboratory. In these cases, an AVS# is assigned for internal record keeping and increased rigor and reproducibility purposes.

Table S2. Lifespan assays data of representative experiments in figures and additional trials.

Figure/ Trials	Strain / Genotype	Median Survival	Total animals (n number)	95% CI of ratio	*P* value compared to WT	Significance
Fig. 1A Trial 1	AVS543: control	18	175	0.6989 to 1.051	**n/a**	**n/a**
	AVS543: *artEx41 [rab-3p::hpk-1::CFP + pCFJ90 (myo-2p::mCherry)]*	21	195	0.6989 to 1.051	<0.0001	****
Fig. 1A Trial 2	AVS399: *gpIs1 [hsp-16.2p::GFP]*	22	264	0.7557 to 1.112	**n/a**	**n/a**
	AVS399*: gpIs1 [hsp-16.2p::GFP]; artEx33 [rab-3p::hpk-1::CFP +pCFJ90 (myo-2p::mCherry)]*	24	169	0.7557 to 1.112	<0.0001	****
Fig. 1B	AVS609: control	24	175	0.7618 to 1.313	n/a	n/a
	AVS609: *artEx43 [myo-3p::hpk-1 + pCFJ90 (myo-2p::mCherry)] line 1*	24	195	0.7618 to 1.313	0.9304	ns
Fig. 1C	AVS627: control	22	117	0.7541 to 1.326	n/a	n/a
	AVS627: *artEx52 [ges-1p::hpk-1 + pCFJ90 (myo-2p::mCherry)] line 1*	22	82	0.7541 to 1.326	0.3226	ns
Fig. 1D	AVS614: control	21	99	0.7631 to 1.310	n/a	n/a
	AVS614: *artEx48 [dpy-7p::hpk-1 + pCFJ90 (myo-2p::mCherry)] line 1*	21	112	0.7631 to 1.310	0.9304	ns
Fig. 5B	AVS709: control	19	73	0.7253 to 1.379	**n/a**	**n/a**
	AVS709: *artEx62 [tph-1p::hpk-1 + pCFJ90 (myo-2p::mCherry)] line 1*	19	76	0.7253 to 1.379	0.1434	**ns**
Fig. 5E	AVS710: control	15	114	0.7735 to 1.293	**n/a**	**n/a**
	AVS710: *artEx65 [unc-47p::hpk-1 + pCFJ90 (myo-2p::mCherry)] line 1*	15	119	0.7735 to 1.293	0.0074	**

Table S3. Polyglutamine aggregates data of representative experiments in figures and additional trials.

Figure/ Trials	Strain / Genotype	RNAi	Days of adulthood	#Foci/animal (mean)	Total cells (n number)	SEM	*P* value compared to control	Significance
Fig. 2B Line 1	AVS832: *rmIs132 [unc-54p::Q35::YFP] I*	n/a	1	13.43	28	0.45	n/a	n/a
	AVS832: *rmIs132 [unc-54p::Q35::YFP] I*	n/a	2	16.62	21	0.95	n/a	n/a
	AVS832: *rmIs132 [unc-54p::Q35::YFP] I*	n/a	3	26	18	1.15	n/a	n/a
	AVS832: *rmIs132 [unc-54p::Q35::YFP] I; artEx58 [rab-3p::hpk-1::CFP + pCFJ90 (myo-2p::mCherry)]*	n/a	1	11.73	22	0.4798	0.013	*
	AVS832: *rmIs132 [unc-54p::Q35::YFP] I; artEx58 [rab-3p::hpk-1::CFP + pCFJ90 (myo-2p::mCherry)]*	n/a	2	14.11	19	0.5181	0.0303	*
	AVS832: *rmIs132 [unc-54p::Q35::YFP] I; artEx58 [rab-3p::hpk-1::CFP + pCFJ90 (myo-2p::mCherry)]*	n/a	3	21.29	24	0.9178	0.0024	**
Fig. 2B Line 2	AVS833: *rmIs132 [unc-54p::Q35::YFP] I*	n/a	1	12.19	21	0.646	n/a	n/a
	AVS833: *rmIs132 [unc-54p::Q35::YFP] I*	n/a	2	22.18	11	1.102	n/a	n/a
	AVS833: *rmIs132 [unc-54p::Q35::YFP] I*	n/a	3	35	18	1.576	n/a	n/a
	AVS833: *rmIs132 [unc-54p::Q35::YFP] I; artEx59 [rab-3p::hpk-1::CFP + pCFJ90 (myo-2p::mCherry)]*	n/a	1	11.05	20	0.59	0.2017	ns

	AVS833: *rmIs132 [unc-54p::Q35::YFP] I; artEx59 [rab-3p::hpk-1::CFP + pCFJ90 (myo-2p::mCherry)]*	n/a	2	16.16	19	0.76	<0.0001	****
	AVS833: *rmIs132 [unc-54p::Q35::YFP] I; artEx59 [rab-3p::hpk-1::CFP + pCFJ90 (myo-2p::mCherry)]*	n/a	3	30.63	24	1.17	0.0282	*
Fig. 2B Line 3	AVS834: *rmIs132 [unc-54p::Q35::YFP] I*	n/a	1	12.91	22	0.75	n/a	n/a
	AVS834: *rmIs132 [unc-54p::Q35::YFP] I*	n/a	2	19.83	23	0.86	n/a	n/a
	AVS834: *rmIs132 [unc-54p::Q35::YFP] I*	n/a	3	28	21	1.26	n/a	n/a
	AVS834: *rmIs132 [unc-54p::Q35::YFP] I; artEx60 [rab-3p::hpk-1::CFP + pCFJ90 (myo-2p::mCherry)]*	n/a	1	10.5	26	0.54	0.0105	*
	AVS834: *rmIs132 [unc-54p::Q35::YFP] I; artEx60 [rab-3p::hpk-1::CFP + pCFJ90 (myo-2p::mCherry)]*	n/a	2	16.12	26	0.69	0.0014	**
	AVS834: *rmIs132 [unc-54p::Q35::YFP] I; artEx60 [rab-3p::hpk-1::CFP + pCFJ90 (myo-2p::mCherry)]*	n/a	3	20.06	31	0.81	<0.0001	****
Fig. 2B Line 4	AVS835: *rmIs132 [unc-54p::Q35::YFP] I*	n/a	1	12.14	21	0.48	n/a	n/a
	AVS835: *rmIs132 [unc-54p::Q35::YFP] I*	n/a	2	20.78	23	0.8	n/a	n/a
	AVS835: *rmIs132 [unc-54p::Q35::YFP] I*	n/a	3	26.79	19	1	n/a	n/a
	AVS835: *rmIs132 [unc-54p::Q35::YFP] I; artEx61 [rab-3p::hpk-1::CFP + pCFJ90 (myo-2p::mCherry)]*	n/a	1	8.593	27	0.507	<0.0001	****
	AVS835: *rmIs132 [unc-54p::Q35::YFP] I; artEx61 [rab-3p::hpk-1::CFP + pCFJ90 (myo-2p::mCherry)]*	n/a	2	16.47	36	0.455	<0.0001	****
	AVS835: *rmIs132 [unc-54p::Q35::YFP] I; artEx61 [rab-3p::hpk-1::CFP + pCFJ90 (myo-2p::mCherry)]*	n/a	3	21.58	33	0.903	0.0005	***
Fig. 2B Line 5	AVS562: *rmIs132 [unc-54p::Q35::YFP] I*	n/a	1	7.185	27	0.453	n/a	n/a
	AVS562: *rmIs132 [unc-54p::Q35::YFP] I*	n/a	2	15.16	32	0.775	n/a	n/a
	AVS562: *rmIs132 [unc-54p::Q35::YFP] I*	n/a	3	28.05	39	0.99	n/a	n/a
	AVS562: *rmIs132 [unc-54p::Q35::YFP] I*	n/a	4	41	25	1.268	n/a	n/a
	AVS562: *rmIs132 [unc-54p::Q35::YFP] I; artEx41 [rab-3p::hpk-1::CFP + pCFJ90 (myo-2p::mCherry)]*	n/a	1	5.409	22	0.495	0.0111	*
	AVS562: *rmIs132 [unc-54p::Q35::YFP] I; artEx41 [rab-3p::hpk-1::CFP + pCFJ90 (myo-2p::mCherry)]*	n/a	2	11.05	20	0.956	0.0017	**
	AVS562: *rmIs132 [unc-54p::Q35::YFP] I; artEx41 [rab-3p::hpk-1::CFP + pCFJ90 (myo-2p::mCherry)]*	n/a	3	21.14	21	0.996	<0.0001	****
	AVS562: *rmIs132 [unc-54p::Q35::YFP] I; artEx41 [rab-3p::hpk-1::CFP + pCFJ90 (myo-2p::mCherry)]*	n/a	4	32.95	21	1.702	0.0004	***
Fig. 2D	AVS540: *rmIs132 [unc-54p::Q35::YFP] I; sid-1(pk3321)V; uIs69[unc-119p::sid-1; myo-2p::mCherry]V*	*empty vector*	1	6.091	22	0.446	n/a	n/a
	AVS540: *rmIs132 [unc-54p::Q35::YFP] I; sid-1(pk3321)V; uIs69[unc-119p::sid-1; myo-2p::mCherry]V*	*empty vector*	2	8.125	24	0.368	n/a	n/a
	AVS540: *rmIs132 [unc-54p::Q35::YFP] I; sid-1(pk3321)V; uIs69[unc-119p::sid-1; myo-2p::mCherry]V*	*empty vector*	3	18.64	25	0.781	n/a	n/a
	AVS540: *rmIs132 [unc-54p::Q35::YFP] I; sid-1(pk3321)V; uIs69[unc-119p::sid-1; myo-2p::mCherry]V*	*empty vector*	4	32.48	29	1.105	n/a	n/a
	AVS540: *rmIs132 [unc-54p::Q35::YFP] I; sid-1(pk3321)V; uIs69[unc-119p::sid-1; myo-2p::mCherry]V*	*hpk-1*	1	7.609	23	0.434	0.0189	*

	AVS540: *rmIs132 [unc-54p::Q35::YFP] I; sid-1(pk3321)V; uIs69[unc-119p::sid-1; myo-2p::mCherry]V*	*hpk-1*	2	12.95	22	0.64	<0.0001	****
	AVS540: *rmIs132 [unc-54p::Q35::YFP] I; sid-1(pk3321)V; uIs69[unc-119p::sid-1; myo-2p::mCherry]V*	*hpk-1*	3	27.12	26	1.209	<0.0001	****
	AVS540: *rmIs132 [unc-54p::Q35::YFP] I; sid-1(pk3321)V; uIs69[unc-119p::sid-1; myo-2p::mCherry]V*	*hpk-1*	4	45.32	28	1.04	<0.0001	****
Fig. 2G,H	AVS562: *rmIs132 [unc-54p::Q35::YFP] I*	n/a	3	28.05	39	0.9898	n/a	n/a
	AVS562: *rmIs132 [unc-54p::Q35::YFP] I; artEx41 [rab-3p::hpk-1::CFP + pCFJ90 (myo-2p::mCherry)]*	n/a	3	21.14	21	0.9959	n/a	n/a
	AVS713: *rmIs132 [unc-54p::Q35::YFP] I; unc-31(e169)V*	n/a	3	21.52	58	0.6527	n/a	n/a
	AVS713: *rmIs132 [unc-54p::Q35::YFP] I; artEx41(rab-3p::hpk-1::CFP + pCFJ90 (myo-2p::mCherry)]; unc-31(e169)V*	n/a	3	18.02	50	0.5859	Compared to AVS713 control: 0.0001	***
	AVS810*rmIs132 [unc-54p::Q35::YFP] I; unc-13(e51)I*	n/a	3	57.81	26	1.098	n/a	n/a
	AVS810*rmIs132 [unc-54p::Q35::YFP] I; artEx41 [rab-3p::hpk-1::CFP + pCFJ90 (myo-2p::mCherry)]; unc-13(e51)I*	n/a	3	58.68	25	1.408	Compared to AVS810 control: 0.6258	ns
Fig. 4A Line 1	AVS682: *rmIs132 [unc-54p::Q35::YFP] I*	n/a	1	6.563	32	0.301	n/a	n/a
	AVS682: *rmIs132 [unc-54p::Q35::YFP] I*	n/a	2	17.43	30	0.7786	n/a	n/a
	AVS682: *rmIs132 [unc-54p::Q35::YFP] I*	n/a	3	40.23	26	1.017	n/a	n/a
	AVS682: *artEx62 [tph-1p::hpk-1 + pCFJ90 (myo-2p::mCherry)] line 1; rmIs132 [unc-54p::Q35::YFP] I*	n/a	1	5.333	21	0.252	0.0056	**
	AVS682: *artEx62 [tph-1p::hpk-1 + pCFJ90 (myo-2p::mCherry)] line 1; rmIs132 [unc-54p::Q35::YFP] I*	n/a	2	15.24	25	0.609	0.0359	*
	AVS682: *artEx62 [tph-1p::hpk-1 + pCFJ90 (myo-2p::mCherry)] line 1; rmIs132 [unc-54p::Q35::YFP] I*	n/a	3	37.06	17	1.152	0.0494	*
Fig. 4A Line 2	AVS683: *rmIs132 [unc-54p::Q35::YFP] I*	n/a	3	31.43	21	1.245	n/a	n/a
	AVS683: *artEx63 [tph-1p::hpk-1 + pCFJ90 (myo-2p::mCherry)] line 1; rmIs132 [unc-54p::Q35::YFP] I*	n/a	3	26.29	24	1.182	0.0046	**
Fig. 4C Line 1	AVS685: *rmIs132 [unc-54p::Q35::YFP] I*	n/a	1	6.737	19	0.3734	n/a	n/a
	AVS685: *rmIs132 [unc-54p::Q35::YFP] I*	n/a	2	12.26	19	0.696	n/a	n/a
	AVS685: *rmIs132 [unc-54p::Q35::YFP] I*	n/a	3	29.67	21	0.9394	n/a	n/a
	AVS685: *artEx65 [unc-47p::hpk-1 + pCFJ90 (myo-2p::mCherry)] line 1; rmIs132 [unc-54p::Q35::YFP] I*	n/a	1	6	25	0.2449	0.0937	ns
	AVS685: *artEx65 [unc-47p::hpk-1 + pCFJ90 (myo-2p::mCherry)] line 1; rmIs132 [unc-54p::Q35::YFP] I*	n/a	2	10.32	25	0.7158	0.064	ns
	AVS685: *artEx65 [unc-47p::hpk-1 + pCFJ90 (myo-2p::mCherry)] line 1; rmIs132 [unc-54p::Q35::YFP] I*	n/a	3	25.5	26	0.8931	0.0026	**
Fig. 4C Line 2	AVS686: *rmIs132 [unc-54p::Q35::YFP] I*	n/a	3	37.32	22	1.223	n/a	n/a
	AVS686: *artEx66 [unc-47p::hpk-1 + pCFJ90 (myo-2p::mCherry)] line 1; rmIs132 [unc-54p::Q35::YFP] I*	n/a	3	33.32	22	1.058	0.0175	*
Fig. S2A Line 1	AVS691: *rmIs132 [unc-54p::Q35::YFP] I*	n/a	1	6.44	25	0.2242	n/a	n/a
	AVS691: *rmIs132 [unc-54p::Q35::YFP] I*	n/a	2	10	32	0.4283	n/a	n/a

	AVS691: *rmIs132 [unc-54p::Q35::YFP] I*	n/a	3	29.6	20	1.663	n/a	n/a
	AVS691: *artEx71 [eat-4p::hpk-1 + pCFJ90 (myo-2p::mCherry)] line 1; rmIs132 [unc-54p::Q35::YFP] I*	n/a	1	5.444	18	0.2826	0.0079	**
	AVS691: *artEx71 [eat-4p::hpk-1 + pCFJ90 (myo-2p::mCherry)] line 1; rmIs132 [unc-54p::Q35::YFP] I*	n/a	2	10.1	21	0.5811	0.8935	ns
	AVS691: *artEx71 [eat-4p::hpk-1 + pCFJ90 (myo-2p::mCherry)] line 1; rmIs132 [unc-54p::Q35::YFP] I*	n/a	3	28.48	23	1.204	0.5812	ns
Fig. S2A Line 2	AVS692: *rmIs132 [unc-54p::Q35::YFP] I*	n/a	3	23.73	22	1.273	n/a	n/a
	AVS692: *artEx72 [eat-4p::hpk-1 + pCFJ90 (myo-2p::mCherry)] line 1; rmIs132 [unc-54p::Q35::YFP] I*	n/a	3	22.64	22	1.118	0.523	ns
Fig. S2C Line 1	AVS693: *rmIs132 [unc-54p::Q35::YFP] I*	n/a	1	6.906	36	0.1871	n/a	n/a
	AVS693: *rmIs132 [unc-54p::Q35::YFP] I*	n/a	2	12.77	26	0.6801	n/a	n/a
	AVS693: *rmIs132 [unc-54p::Q35::YFP] I*	n/a	3	32.88	33	0.7986	n/a	n/a
	AVS693: *artEx73 [cat-2p::hpk-1 + pCFJ90 (myo-2p::mCherry)] line 1; rmIs132 [unc-54p::Q35::YFP] I*	n/a	1	7.563	16	0.3648	0.0816	ns
	AVS693: *artEx73 [cat-2p::hpk-1 + pCFJ90 (myo-2p::mCherry)] line 1; rmIs132 [unc-54p::Q35::YFP] I*	n/a	2	12.15	20	0.8088	0.5587	ns
	AVS693: *artEx73 [cat-2p::hpk-1 + pCFJ90 (myo-2p::mCherry)] line 1; rmIs132 [unc-54p::Q35::YFP] I*	n/a	3	33.21	24	1.07	0.8019	ns
Fig. S2C Line 2	AVS694: *rmIs132 [unc-54p::Q35::YFP] I*	n/a	3	22.64	22	1.118	n/a	n/a
	AVS694: *artEx74 [cat-2p::hpk-1 + pCFJ90 (myo-2p::mCherry)] line 1; rmIs132 [unc-54p::Q35::YFP] I*	n/a	3	23.73	22	1.273	0.574	ns

Table S4. Body bends assay data.

Figure/ Trials	Strain / Genotype	RNAi	Body bends mean (30 seconds)	Total animals (n number)	SEM	*P* value compared to control	Significance
Fig. 1E	N2: *wild type*	n/a	48.72	40	0.7938	n/a	n/a
	AVS392: *hpk-1(pk1393)*	n/a	27.35	41	1.047	<0.0001	****
	AVS420: *hpk-1(pk1393) X; artEx41 [rab-3p::hpk-1::CFP + pCFJ90 (myo-2p::mCherry)]*	n/a	36.22	50	1.323	Compared to *hpk-1(pk1393)*: <0.0001	****

Table S5. Paralysis assay data of representative experiments in figures and additional trials.

Figure/ Trials	Strain / Genotype	RNAi	Days of adulthood	% of paralyzed animals	Total cells (n number)	SEM	*P* value compared to control	Significance
Fig. 2C Line 1	AVS832: *rmIs132 [unc-54p::Q35::YFP] I*	n/a	5	0%	27	0	**n/a**	**n/a**
	AVS832: *rmIs132 [unc-54p::Q35::YFP] I*	n/a	7	11%	27	0.06163	**n/a**	**n/a**
	AVS832: *rmIs132 [unc-54p::Q35::YFP] I*	n/a	9	33%	27	0.09245	**n/a**	**n/a**
	AVS832: *rmIs132 [unc-54p::Q35::YFP] I*	n/a	11	56%	27	0.09745	**n/a**	**n/a**

	AVS832: *rmIs132 [unc-54p::Q35::YFP] I*	n/a	13	81%	27	0.07618	**n/a**	**n/a**
	AVS832: *rmIs132 [unc-54p::Q35::YFP] I; artEx58 [rab-3p::hpk-1::CFP + pCFJ90 (myo-2p::mCherry)]*	n/a	5	0%	23	0	**n/a**	**n/a**
	AVS832: *rmIs132 [unc-54p::Q35::YFP] I; artEx58 [rab-3p::hpk-1::CFP + pCFJ90 (myo-2p::mCherry)]*	n/a	7	0%	23	0	0.1032	ns
	AVS832: *rmIs132 [unc-54p::Q35::YFP] I; artEx58 [rab-3p::hpk-1::CFP + pCFJ90 (myo-2p::mCherry)]*	n/a	9	17%	23	0.08081	0.2081	ns
	AVS832: *rmIs132 [unc-54p::Q35::YFP] I; artEx58 [rab-3p::hpk-1::CFP + pCFJ90 (myo-2p::mCherry)]*	n/a	11	43%	23	0.1057	0.405	ns
	AVS832: *rmIs132 [unc-54p::Q35::YFP] I; artEx58 [rab-3p::hpk-1::CFP + pCFJ90 (myo-2p::mCherry)]*	n/a	13	61%	23	0.1041	0.11	ns
Fig. 2C Line 2	AVS833: *rmIs132 [unc-54p::Q35::YFP] I*	n/a	5	0%	28	0	n/a	n/a
	AVS833: *rmIs132 [unc-54p::Q35::YFP] I*	n/a	7	21%	28	0.07897	n/a	n/a
	AVS833: *rmIs132 [unc-54p::Q35::YFP] I*	n/a	9	43%	28	0.09524	n/a	n/a
	AVS833: *rmIs132 [unc-54p::Q35::YFP] I*	n/a	11	79%	28	0.07897	n/a	n/a
	AVS833: *rmIs132 [unc-54p::Q35::YFP] I*	n/a	13	89%	28	0.05952	n/a	n/a
	AVS833: *rmIs132 [unc-54p::Q35::YFP] I; artEx59 [rab-3p::hpk-1::CFP + pCFJ90 (myo-2p::mCherry)]*	n/a	5	0%	20	0	n/a	n/a
	AVS833: *rmIs132 [unc-54p::Q35::YFP] I; artEx59 [rab-3p::hpk-1::CFP + pCFJ90 (myo-2p::mCherry)]*	n/a	7	5%	20	0.05	0.1166	ns
	AVS833: *rmIs132 [unc-54p::Q35::YFP] I; artEx59 [rab-3p::hpk-1::CFP + pCFJ90 (myo-2p::mCherry)]*	n/a	9	30%	20	0.1051	0.3751	ns
	AVS833: *rmIs132 [unc-54p::Q35::YFP] I; artEx59 [rab-3p::hpk-1::CFP + pCFJ90 (myo-2p::mCherry)]*	n/a	11	65%	20	0.1094	0.307	ns
	AVS833: *rmIs132 [unc-54p::Q35::YFP] I; artEx59 [rab-3p::hpk-1::CFP + pCFJ90 (myo-2p::mCherry)]*	n/a	13	80%	20	0.09177	0.3796	ns
Fig. 2C Line 3	AVS834: *rmIs132 [unc-54p::Q35::YFP] I*	n/a	5	0%	28	0	n/a	n/a
	AVS834: *rmIs132 [unc-54p::Q35::YFP] I*	n/a	7	3%	28	0.03571	n/a	n/a
	AVS834: *rmIs132 [unc-54p::Q35::YFP] I*	n/a	9	3%	28	0.03571	n/a	n/a
	AVS834: *rmIs132 [unc-54p::Q35::YFP] I*	n/a	11	39%	28	0.09399	n/a	n/a
	AVS834: *rmIs132 [unc-54p::Q35::YFP] I*	n/a	13	60%	28	0.09399	n/a	n/a
	AVS834: *rmIs132 [unc-54p::Q35::YFP] I; artEx60 [rab-3p::hpk-1::CFP + pCFJ90 (myo-2p::mCherry)]*	n/a	5	0%	22	0	n/a	n/a
	AVS834: *rmIs132 [unc-54p::Q35::YFP] I; artEx60 [rab-3p::hpk-1::CFP + pCFJ90 (myo-2p::mCherry)]*	n/a	7	5%	22	0.04545	0.8649	ns
	AVS834: *rmIs132 [unc-54p::Q35::YFP] I; artEx60 [rab-3p::hpk-1::CFP + pCFJ90 (myo-2p::mCherry)]*	n/a	9	5%	22	0.04545	0.8649	ns
	AVS834: *rmIs132 [unc-54p::Q35::YFP] I; artEx60 [rab-3p::hpk-1::CFP + pCFJ90 (myo-2p::mCherry)]*	n/a	11	23%	22	0.09145	0.2209	ns
	AVS834: *rmIs132 [unc-54p::Q35::YFP] I; artEx60 [rab-3p::hpk-1::CFP + pCFJ90 (myo-2p::mCherry)]*	n/a	13	41%	22	0.1073	0.1708	ns
Fig. 2C Line 4	AVS835: *rmIs132 [unc-54p::Q35::YFP] I*	n/a	5	0%	25	0	n/a	n/a
	AVS835: *rmIs132 [unc-54p::Q35::YFP] I*	n/a	7	0%	25	0	n/a	n/a

	AVS835: *rmIs132 [unc-54p::Q35::YFP] I*	n/a	9	20%	25	0.8165	n/a	n/a
	AVS835: *rmIs132 [unc-54p::Q35::YFP] I*	n/a	11	60%	25	0.1	n/a	n/a
	AVS835: *rmIs132 [unc-54p::Q35::YFP] I*	n/a	13	60%	25	0.1	n/a	n/a
	AVS835: *rmIs132 [unc-54p::Q35::YFP] I; artEx61 [rab-3p::hpk-1::CFP + pCFJ90 (myo-2p::mCherry)]*	n/a	5	0%	24	0	n/a	n/a
	AVS835: *rmIs132 [unc-54p::Q35::YFP] I; artEx61 [rab-3p::hpk-1::CFP + pCFJ90 (myo-2p::mCherry)]*	n/a	7	0%	24	0	n/a	n/a
	AVS835: *rmIs132 [unc-54p::Q35::YFP] I; artEx61 [rab-3p::hpk-1::CFP + pCFJ90 (myo-2p::mCherry)]*	n/a	9	4%	24	0.04167	0.0946	ns
	AVS835: *rmIs132 [unc-54p::Q35::YFP] I; artEx61 [rab-3p::hpk-1::CFP + pCFJ90 (myo-2p::mCherry)]*	n/a	11	38%	24	0.1009	0.1201	ns
	AVS835: *rmIs132 [unc-54p::Q35::YFP] I; artEx61 [rab-3p::hpk-1::CFP + pCFJ90 (myo-2p::mCherry)]*	n/a	13	54%	24	0.1039	0.6876	ns
Fig. 2C Line 5	AVS562: *rmIs132 [unc-54p::Q35::YFP] I*	n/a	3	0%	54	0	n/a	n/a
	AVS562: *rmIs132 [unc-54p::Q35::YFP] I*	n/a	5	2%	54	0.01852	n/a	n/a
	AVS562: *rmIs132 [unc-54p::Q35::YFP] I*	n/a	7	4%	54	0.02594	n/a	n/a
	AVS562: *rmIs132 [unc-54p::Q35::YFP] I*	n/a	9	69%	54	0.0638	n/a	n/a
	AVS562: *rmIs132 [unc-54p::Q35::YFP] I; artEx41 [rab-3p::hpk-1::CFP + pCFJ90 (myo-2p::mCherry)]*	n/a	3	0%	50	0	n/a	n/a
	AVS562: *rmIs132 [unc-54p::Q35::YFP] I; artEx41 [rab-3p::hpk-1::CFP + pCFJ90 (myo-2p::mCherry)]*	n/a	5	2%	50	0.02	0.9567	ns
	AVS562: *rmIs132 [unc-54p::Q35::YFP] I; artEx41 [rab-3p::hpk-1::CFP + pCFJ90 (myo-2p::mCherry)]*	n/a	7	4%	50	0.028	0.9382	ns
	AVS562: *rmIs132 [unc-54p::Q35::YFP] I; artEx41 [rab-3p::hpk-1::CFP + pCFJ90 (myo-2p::mCherry)]*	n/a	9	38%	50	0.0808	0.0034	**
Fig. 2E	AVS540: *rmIs132 [unc-54p::Q35::YFP] I; sid-1(pk3321)V; uIs69[unc-119p::sid-1; myo-2p::mCherry]V*	*empty vector*	3	0%	78	0	n/a	n/a
	AVS540: *rmIs132 [unc-54p::Q35::YFP] I; sid-1(pk3321)V; uIs69[unc-119p::sid-1; myo-2p::mCherry]V*	*empty vector*	5	0%	78	0	n/a	n/a
	AVS540: *rmIs132 [unc-54p::Q35::YFP] I; sid-1(pk3321)V; uIs69[unc-119p::sid-1; myo-2p::mCherry]V*	*empty vector*	7	5%	78	0.02514	n/a	n/a
	AVS540: *rmIs132 [unc-54p::Q35::YFP] I; sid-1(pk3321)V; uIs69[unc-119p::sid-1; myo-2p::mCherry]V*	*empty vector*	9	13%	78	0.04052	n/a	n/a
	AVS540: *rmIs132 [unc-54p::Q35::YFP] I; sid-1(pk3321)V; uIs69[unc-119p::sid-1; myo-2p::mCherry]V*	*empty vector*	11	23%	78	0.04801	n/a	n/a
	AVS540: *rmIs132 [unc-54p::Q35::YFP] I; sid-1(pk3321)V; uIs69[unc-119p::sid-1; myo-2p::mCherry]V*	*hpk-1*	3	0%	73	0	n/a	n/a
	AVS540: *rmIs132 [unc-54p::Q35::YFP] I; sid-1(pk3321)V; uIs69[unc-119p::sid-1; myo-2p::mCherry]V*	*hpk-1*	5	8%	73	0.03237	0.0096	**
	AVS540: *rmIs132 [unc-54p::Q35::YFP] I; sid-1(pk3321)V; uIs69[unc-119p::sid-1; myo-2p::mCherry]V*	*hpk-1*	7	33%	73	0.05536	<0.0001	****
	AVS540: *rmIs132 [unc-54p::Q35::YFP] I; sid-1(pk3321)V; uIs69[unc-119p::sid-1; myo-2p::mCherry]V*	*hpk-1*	9	84%	73	0.04368	<0.0001	****
	AVS540: *rmIs132 [unc-54p::Q35::YFP] I; sid-1(pk3321)V; uIs69[unc-119p::sid-1; myo-2p::mCherry]V*	*hpk-1*	11	95%	73	0.02682	<0.0001	****
Fig. 4B	AVS682: *rmIs132 [unc-54p::Q35::YFP] I*	n/a	5	0%	30	0	n/a	n/a

	AVS682: *rmIs132 [unc-54p::Q35::YFP] I*	n/a	7	23%	30	0.07854	n/a	n/a
	AVS682: *rmIs132 [unc-54p::Q35::YFP] I*	n/a	9	53%	30	0.09264	n/a	n/a
	AVS682: *rmIs132 [unc-54p::Q35::YFP] I*	n/a	11	93%	30	0.04632	n/a	n/a
	AVS682: *artEx62 [tph-1p::hpk-1 + pCFJ90 (myo-2p::mCherry)] line 1; rmIs132 [unc-54p::Q35::YFP] I*	n/a	5	0%	28	0	n/a	n/a
	AVS682: *artEx62 [tph-1p::hpk-1 + pCFJ90 (myo-2p::mCherry)] line 1; rmIs132 [unc-54p::Q35::YFP] I*	n/a	7	11%	28	0.05952	0.2104	ns
	AVS682: *artEx62 [tph-1p::hpk-1 + pCFJ90 (myo-2p::mCherry)] line 1; rmIs132 [unc-54p::Q35::YFP] I*	n/a	9	39%	28	0.09399	0.292	ns
	AVS682: *artEx62 [tph-1p::hpk-1 + pCFJ90 (myo-2p::mCherry)] line 1; rmIs132 [unc-54p::Q35::YFP] I*	n/a	11	75%	28	0.08333	0.0553	ns
Fig. 4D	AVS685: *rmIs132 [unc-54p::Q35::YFP] I*	n/a	5	0%	27	0	n/a	n/a
	AVS685: *rmIs132 [unc-54p::Q35::YFP] I*	n/a	7	19%	27	0.07618	n/a	n/a
	AVS685: *rmIs132 [unc-54p::Q35::YFP] I*	n/a	9	56%	27	0.09745	n/a	n/a
	AVS685: *rmIs132 [unc-54p::Q35::YFP] I*	n/a	11	93%	27	0.05136	n/a	n/a
	AVS685: *artEx65 [unc-47p::hpk-1 + pCFJ90 (myo-2p::mCherry)] line 1; rmIs132 [unc-54p::Q35::YFP] I*	n/a	5	0%	28	0	n/a	n/a
	AVS685: *artEx65 [unc-47p::hpk-1 + pCFJ90 (myo-2p::mCherry)] line 1; rmIs132 [unc-54p::Q35::YFP] I*	n/a	7	18%	28	0.1786	0.9505	ns
	AVS685: *artEx65 [unc-47p::hpk-1 + pCFJ90 (myo-2p::mCherry)] line 1; rmIs132 [unc-54p::Q35::YFP] I*	n/a	9	50%	28	0.09623	0.6867	ns
	AVS685: *artEx65 [unc-47p::hpk-1 + pCFJ90 (myo-2p::mCherry)] line 1; rmIs132 [unc-54p::Q35::YFP] I*	n/a	11	79%	28	0.07897	0.1456	ns
Fig. S2B	AVS691: *rmIs132 [unc-54p::Q35::YFP] I*	n/a	5	0%	33	0	n/a	n/a
	AVS691: *rmIs132 [unc-54p::Q35::YFP] I*	n/a	7	18%	33	0.06818	n/a	n/a
	AVS691: *rmIs132 [unc-54p::Q35::YFP] I*	n/a	9	42%	33	0.08737	n/a	n/a
	AVS691: *rmIs132 [unc-54p::Q35::YFP] I*	n/a	11	88%	33	0.0577	n/a	n/a
	AVS691: *artEx71 [eat-4p::hpk-1 + pCFJ90 (myo-2p::mCherry)] line 1; rmIs132 [unc-54p::Q35::YFP] I*	n/a	5	0%	29	0	n/a	n/a
	AVS691: *artEx71 [eat-4p::hpk-1 + pCFJ90 (myo-2p::mCherry)] line 1; rmIs132 [unc-54p::Q35::YFP] I*	n/a	7	14%	29	0.06517	0.6458	ns
	AVS691: *artEx71 [eat-4p::hpk-1 + pCFJ90 (myo-2p::mCherry)] line 1; rmIs132 [unc-54p::Q35::YFP] I*	n/a	9	41%	29	0.09308	0.935	ns
	AVS691: *artEx71 [eat-4p::hpk-1 + pCFJ90 (myo-2p::mCherry)] line 1; rmIs132 [unc-54p::Q35::YFP] I*	n/a	11	83%	29	0.07139	0.5754	ns
Fig. S2D	AVS693: *rmIs132 [unc-54p::Q35::YFP] I*	n/a	5	0%	34	0	n/a	n/a
	AVS693: *rmIs132 [unc-54p::Q35::YFP] I*	n/a	7	15%	34	0.06165	n/a	n/a
	AVS693: *rmIs132 [unc-54p::Q35::YFP] I*	n/a	9	44%	34	0.08643	n/a	n/a
	AVS693: *rmIs132 [unc-54p::Q35::YFP] I*	n/a	11	88%	34	0.05609	n/a	n/a

	AVS693: *artEx73 [cat-2p::hpk-1 + pCFJ90 (myo-2p::mCherry)] line 1; rmIs132 [unc-54p::Q35::YFP] I*	n/a	5	0%	35	0	n/a	n/a
	AVS693: *artEx73 [cat-2p::hpk-1 + pCFJ90 (myo-2p::mCherry)] line 1; rmIs132 [unc-54p::Q35::YFP] I*	n/a	7	11%	35	0.05456	0.6914	ns
	AVS693: *artEx73 [cat-2p::hpk-1 + pCFJ90 (myo-2p::mCherry)] line 1; rmIs132 [unc-54p::Q35::YFP] I*	n/a	9	40%	35	0.08402	0.7337	ns
	AVS693: *artEx73 [cat-2p::hpk-1 + pCFJ90 (myo-2p::mCherry)] line 1; rmIs132 [unc-54p::Q35::YFP] I*	n/a	11	83%	35	0.06463	0.5328	ns

Table S6. Thermotolerance assay data of all representative experiments in figures and other trials.

Figure/ Trials	Strain / Genotype	Exposure time at 35C	Survival %	Total animals (n number)	SEM	*P* value compared to control	Significance
Fig. 1F Trial 1	N2	10h	80%	220	0.0268	n/a	n/a
	hpk-1(pk1393) X	10h	48%	27	0.09799	<0.0001	****
	hpk-1(pk1393) X; artEx41 [rab-3p::hpk-1::CFP + pCFJ90 (myo-2p::mCherry)]	10h	82%	50	0.05488	Compared to *hpk-1(pk1393):* 0.0016	**
Fig. 1F Trial 2	N2	10h	64%	130	0.00251	n/a	n/a
	hpk-1(pk1393) X	10h	27%	66	0.01088	<0.0001	****
	hpk-1(pk1393) X; artEx41 [rab-3p::hpk-1::CFP + pCFJ90 (myo-2p::mCherry)]	10h	76%	75	0.00965	Compared to *hpk-1(pk1393):* <0.0001	****
Fig. 5A	AVS709: control	6h	84%	32	0.06521	n/a	n/a
	AVS709: control	8h	67%	39	0.07647	n/a	n/a
	AVS709: *artEx62 [tph-1p::hpk-1 + pCFJ90 (myo-2p::mCherry)] line 1*	6h	100%	33	0	0.0178	*
	AVS709: *artEx62 [tph-1p::hpk-1 + pCFJ90 (myo-2p::mCherry)] line 1*	8h	83%	41	0.05949	0.0955	ns
Fig. 5D	AVS710: control	6h	85%	54	0.0488	n/a	n/a
	AVS710: control	8h	69%	49	0.6652	n/a	n/a
	AVS710: *artEx65 [unc-47p::hpk-1 + pCFJ90 (myo-2p::mCherry)] line 1*	6h	89%	47	0.04546	0.5366	ns
	AVS710: *artEx65 [unc-47p::hpk-1 + pCFJ90 (myo-2p::mCherry)] line 1*	8h	69%	51	0.06562	0.9353	ns

Table S7. Induction of *hsp-16.2p::GFP* data after heat stress.

Figure/ Trials	Strain / Genotype	Conditions	GFP a.u.	Total animals (n number)	SEM	*P* value compared to control	Significance
Fig. 3B Trial 1	AVS399: *gpIs1 [hsp-16.2p::GFP]*	Heat shock 1hr at 35C, 2hr recovery at 20C	719.6	15	31.8	n/a	n/a
	AVS399: *gpIs1 [hsp-16.2p::GFP]; artEx33 [rab-3p::hpk-1::CFP +pCFJ90 (myo-2p::mCherry)]*	Heat shock 1hr at 35C, 2hr recovery at 20C	845.9	25	42.3	0.0422	*
Fig. 3B Trial 2	AVS399: *gpIs1 [hsp-16.2p::GFP]*	Heat shock 1hr at 30C, 2hr recovery at 20C	27.27	19	3.827	n/a	n/a
	AVS399: *gpIs1 [hsp-16.2p::GFP]; artEx33 [rab-3p::hpk-1::CFP +pCFJ90 (myo-2p::mCherry)]*	Heat shock 1hr at 30C, 2hr recovery at 20C	44.79	13	8.523	0.0456	*
Fig. S1C Trial 1	AVS399: *gpIs1 [hsp-16.2p::GFP]*	Heat shock 1hr at 35C, 2hr recovery at 20C	975.9	14	28.1	n/a	n/a
	AVS399: *gpIs1 [hsp-16.2p::GFP]; artEx33 [rab-3p::hpk-1::CFP +pCFJ90 (myo-2p::mCherry)]*	Heat shock 1hr at 35C, 2hr recovery at 20C	937.7	24	58.01	0.6324	ns

Fig. S1C Trial 2	AVS399: *gpIs1 [hsp-16.2p::GFP]*	Heat shock 1hr at 30C, 2hr recovery at 20C	15.26	19	1.772	0.0178	*
	AVS399: *gpIs1 [hsp-16.2p::GFP]; artEx33 [rab-3p::hpk-1::CFP +pCFJ90 (myo-2p::mCherry)]*	Heat shock 1hr at 30C, 2hr recovery at 20C	13.46	14	1.719	0.4837	ns

Table S8. Induction of autophagosomes at basal conditions data.

Figure/ Trials	Strain / Genotype	Age	# of autophagosomes	Total cells (n number)	SEM	*P* value compared to control	Significance
Fig. 3D Trial 1	AVS716: *sqIs13 [lgg-1p::GFP::lgg-1 + odr-1p::RFP]*	L4	1.576	59	0.1214	n/a	n/a
	AVS716: *artEx41 [rab-3p::hpk-1::CFP + pCFJ90 (myo-2p::mCherry)]; sqIs13 [lgg-1p::GFP::lgg-1 + odr-1p::RFP]*	L4	2.651	43	0.166	<0.0001	****
Fig. 3D Trial 2	AVS716: *sqIs13 [lgg-1p::GFP::lgg-1 + odr-1p::RFP]*	L4	1.863	80	0.1107	n/a	n/a
	AVS716: *sqIs13 [lgg-1p::GFP::lgg-1 + odr-1p::RFP]*	D1	2.597	67	0.1295	n/a	n/a
	AVS716: *artEx41 [rab-3p::hpk-1::CFP + pCFJ90 (myo-2p::mCherry)]; sqIs13 [lgg-1p::GFP::lgg-1 + odr-1p::RFP]*	L4	2.418	79	0.1355	0.0018	**
	AVS716: *artEx41 [rab-3p::hpk-1::CFP + pCFJ90 (myo-2p::mCherry)]; sqIs13 [lgg-1p::GFP::lgg-1 + odr-1p::RFP]*	D1	3.574	61	0.1661	<0.0001	****
Fig. 5C	AVS809: *sqIs13 [lgg-1p::GFP::lgg-1 + odr-1p::RFP]*	D1	1.238	80	0.09285	n/a	n/a
	AVS809: *artEx62 [tph-1p::hpk-1 + pCFJ90 (myo-2p::mCherry)] line 1; sqIs13 [lgg-1p::GFP::lgg-1 + odr-1p::RFP]*	D1	1.356	104	0.08074	0.3372	ns
Fig. 5F	AVS794: *sqIs13 [lgg-1p::GFP::lgg-1 + odr-1p::RFP]*	D1	1.672	64	0.1221	n/a	n/a
	AVS794: *artEx65 [unc-47p::hpk-1 + pCFJ90 (myo-2p::mCherry)] line 1; sqIs13 [lgg-1p::GFP::lgg-1 + odr-1p::RFP]*	D1	2.329	73	0.1051	<0.0001	****
Fig. S1E Trial 1	AVS716: *sqIs13 [lgg-1p::GFP::lgg-1 + odr-1p::RFP]*	L4	21	11	2.347	n/a	n/a
	AVS716: *artEx41 [rab-3p::hpk-1::CFP + pCFJ90 (myo-2p::mCherry)]; sqIs13 [lgg-1p::GFP::lgg-1 + odr-1p::RFP]*	L4	19	11	2.106	0.5331	ns
Fig. S1E Trial 2	AVS716: *sqIs13 [lgg-1p::GFP::lgg-1 + odr-1p::RFP]*	L4	23.57	23	2.51	n/a	n/a
	AVS716: *artEx41 [rab-3p::hpk-1::CFP + pCFJ90 (myo-2p::mCherry)]; sqIs13 [lgg-1p::GFP::lgg-1 + odr-1p::RFP]*	L4	21.35	17	3.313	0.5905	ns
Fig. 5G	AVS872: *sqIs24 [lgg-1p::GFP::lgg-1 + unc-122p::RFP]; tph-1(mg280)*	D1	1	73	0.1068	n/a	n/a
	AVS872: *artEx41(rab-3p::hpk-1::CFP + pCFJ90 (myo-2p::mCherry); sqIs24 [lgg-1p::GFP::lgg-1 + unc-122p::RFP]; tph-1(mg280)*	D1	2.04	67	0.1465	<0.0001	****
	AVS816: *sqIs24 [lgg-1p::GFP::lgg-1 + unc-122p::RFP]; unc-30(ok613)*	D1	1.36	75	0.1033	n/a	n/a
	AVS816: *artEx41(rab-3p::hpk-1::CFP + pCFJ90 (myo-2p::mCherry); sqIs24 [lgg-1p::GFP::lgg-1 + unc-122p::RFP]; unc-30(ok613)*	D1	1.35	83	0.1229	0.9480	ns